https://doi.org/10.5194/egusphere-2022-1183
Preprint. Discussion started: 12 December 2022

Structural control of inherited salt structures during inversion of a domino basement-fault system from an analogue modelling approach

Oriol Ferrer[1,2], Eloi Carola[1,2], Ken McClay[3,4]

[1]Institut de Recerca Geomodels - UB, Facultat de Ciències de la Terra, Universitat de Barcelona (UB), C/ Martí i Franquès s/n, 08028 Barcelona, Spain.
[2]Departament de Dinàmica de la Terra i de l´Oceà, GRC Geodinàmica i Anàlisi de Conca (GGAC), Facultat de Ciències de la Terra, Universitat de Barcelona (UB), C/ Martí i Franquès s/n, 08028 Barcelona, Spain.
[3]Australian School of Petroleum and Energy Resources, University of Adelaide, South Australia, 5005 Australia.
[4]Earth Sciences Department, Royal Holloway University of London, Egham, Surrey TW20 0EX, UK.

Correspondence to: Oriol Ferrer (joferrer@ub.edu)

Abstract. Inversion of an extensional domino-like basement faults system with a pre-extension decoupling layer is presented as a set of analogue models to understand the role of pre-existing structural features during inversion. The present study expands the experimental program by Ferrer et al. (2022a) in which, models were carried out with different salt and overburden thicknesses to investigate the role played by the salt and by the overburden during extension but also, how extensional structures and salt distribution condition the evolution during inversion. The results show that after total inversion of the models, the resultant structural style of deformation is highly influenced by the inherited extensional configuration and by the thickness of salt which they both condition the degree of coupling/decupling between the pre- and syn-kinematic successions. While models with thick salt can partially or totally preserve the extensional ramp-syncline basin geometry independently of the overburden thickness, models with thin salt result in a total inversion of the ramp-syncline basins with the development of crestal collapse grabens and extensional faults affecting the overburden. Compression triggered the development or reactivation of salt-related structures such as primary weld reactivations (i.e., reopening and/or obliteration), diapir rejuvenation, salt thickening, thrust emplacement, etc. The development of these elements is conditioned by the salt thickness distribution at the end of the extension and therefore, a precise understanding of inherited salt-related structures in needed so to understand the inversion of the basin as well as characterise the structural style.

Introduction

Resultant geometries from basin inversion are highly conditioned by the inherited structural and stratigraphic elements but also by the tectono-sedimentary evolution through time (Nemčok et al., 1995; Turner and Williams, 2004; Panien et al., 2005; Bonini et al., 2012; Lacombe and Bellahsen, 2016;). In inverted rift systems, it is common the presence of broad anticlines at the hanging wall of the major basement faults made up of either post-extension or syn-inversion rocks that in turn are cored by thickened syn-extensional or evaporitic successions (Fig. 1) (e.g., Badley et al., 1989; Gowers et al., 1993; Bonini et al., 2012; Jagger and McClay, 2018; Hansen et al., 2021). These geometries are highly conditioned by the degree of linkage between

https://doi.org/10.5194/egusphere-2022-1183
Preprint. Discussion started: 12 December 2022

the overburden and the basement under extension but also during the inversion of the basins. Among the most important factors conditioning this coupling/decoupling, the location of inherited salt or extensional structures, salt and overburden thicknesses or primary salt welds developed under extension highly impact the reactivation or development of compressional structures and therefore, determine the structural style of deformation (Koyi et al., 1993; Withjack and Callaway, 2000; Withjack et al., 2000; Dooley et al., 2005; Duffy et al., 2013; Ferrer et al., 2014 and 2022a; Carola et al., 2015; Roma et al., 2018a; Coleman et al., 2019; Tari et al., 2020; Dooley and Hudec, 2020; Granado et al., 2021;).

Deformation during rift system inversion is highly controlled by the inherited extensional architecture as well as the location of salt structures and the continuity or disruption of the salt layer (Steward and Clark, 1999; Jackson et al., 2013; Rowan and Krzywiec, 2014). Salt acts as a contractional detachment, with diapirs and salt walls, as the weakest rheological areas of the basin infill, are where deformation is going to be focussed during the early stages of the inversion (Costa and Vendeville, 2002; Brun and Fort, 2004; Callot et al 2007; Dooley et al 2014). Shortening rejuvenates salt structures buried at the end of the extension and salt can extrude forming salt sheets once the overburden is eroded up to the point in which the salt pierces (Jackson and Hudec, 2017). As shortening progresses, diapirs are squeezed developing secondary welds, thrust welds or decapitated diapirs (Dooley et al 2014; Roma et al., 2018b; Vidal-Royo et al., 2021; Rowan et al., 2022).

Analogue modelling investigating the inversion of former extensional basins with isotropic infills has been widely addressed in the literature (i.e., Buchanan and McClay, 1991; Letouzey et al., 1995; Yamada and McClay, 2003; Jagger and McClay, 2018), the number of works of inverted basins with mechanical anisotropies in the sedimentary fill caused by salt layers is scarce (for a detailed review, the reader is addressed to Bonini et al., 2011). While some of them considered pre-rift salt (i.e., Brun and Nalpas, 1996; Withjack and Callaway, 2000; Dooley et al., 2005; Burliga *et al.*, 2012; Ferrer et al., 2016 and 2022a), others investigate the role of syn-rift salt during inversion (i.e., Del Ventisette et al., 2005; Roma et al., 2018a; Dooley and Hudec, 2020). Regardless of when salt was deposited (pre- or syn-extension), most of these works used non-rotational rigid blocs with different geometries and configurations to constrain the geometry of basement faults. Dooley and Hudec (2020) used an original setup based on polymer seed to constrain the geometry of segmented rifts subsequently inverted. The resulting basins were filled with syn-rift evaporites and they analysed the styles of shortening in the sub- and supra-salt section.
The present work complements the experimental program presented by Ferrer et al. (2022a), in which from a systematic set of 2D analogue models simulating an extensional domino-style basement fault system, different parameters controlling the architecture and kinematic of salt-bearing rift basins are studied (i.e., the interplay between pre-kinematic salt and overburden thicknesses, the syn-kinematic sedimentation rate, and the development of primary welds). Taking advantage of the structural templates at the end of the extensional episode in the experiments with a single pre-kinematic salt layer, in this work the positive inversion of these inherited structures is analysed, mainly focusing on how the salt-related structures preferentially localise contractional deformation but also how primary extensional welds are reactivated under compression. The set of extension-inversion models presented in this work allows the direct comparison of salt structures at the end of each deformation stage unravelling the role of the inherited structural grain during the inversion.

https://doi.org/10.5194/egusphere-2022-1183
Preprint. Discussion started: 12 December 2022

Analogue modelling

1.1 Experimental methodology

1.1.1 Experimental program, setup, and procedure

The experimental program was carried out in a rig consisting of five fault blocks simulating a domino fault system (Fig. 2a). ~~Summarizing the rig,~~ it is made up of five metal blocks whose geometry simulates four basement faults (F1 to F4 in Fig. 2a). Four blocks were able to rotate while one was kept fixed at the end of the rig. Each rotation block was attached to a basal trellis system that transmitted the deformation (Fig. 2a). ~~Either~~ extension ~~or~~ compression was applied by an electric motor worm-screw at a velocity ratio of 4.6 mm/h. The sandbox was closed by two lateral glass walls that enabled to record the kinematic evolution of the experiments (Fig. 2a). It should be noted that the design of the rig makes the fault displacement greater in F4 progressively decreasing towards F1. In this way, for a specific experimental configuration, this allows the comparison of equivalent structures with different evolutionary stages for both extension and inversion at each basement block (Fig. 2). For more details, it is suggested to read the work by Ferrer et al. (2022a) where the experimental apparatus is explained in detail.

[Figure 2]

The pre-extensional unit distribution was characterized by a flat basement (provided by each metal block placed horizontally) overlayed by a 30 mm-thick pre-kinematic unit of alternating layers of blue, white, and black silica sand that were levelled with a scraper (e.g., Krantz, 1991; Lohrmann et al., 2003). Transparent polymer (either 5 or 10 mm thick depending on the model, see Table 1) was carefully deposited on top of the quartz sand and the model was left for 24 hours so the polymer flowed attaining a horizontal and constant thickness attitude. The final pre-kinematic cover sand was placed overlying the polymer and alternating 2.5 mm-thick blue, white, and black sand layers flattened with the scrapper up to a total thickness of 7.5 or 15 mm depending on the model (Fig. 2a and Table 1).

[Table 1]

The aim of the experimental program of this study was to understand how the interaction between the thickness of the salt layer and the pre-extensional overburden influenced on the development of salt structures in a domino basement fault system, and how these structures were reactivated and evolved during subsequent inversion. According to that, the four extensional experiments (DOM4, DOM5, DOM6, and DOM8) were subsequently repeated with the same parameters to later apply total inversion (DOM9, DOM12, DOM19, and DOM21 respectively). As a result, the experimental program presented in this work consists of four pairs of extension-inversion models that can be directly compared (Table 1).

At the beginning of the extension, the dip of the four faults limiting the metal blocks was 60º towards the moving wall. As the extension increased, the counterclockwise rotation of the blocks caused the decrease in dip of the fault plane (faults F2, F3, and F4) reaching 50º at the end of the extension (Fig. 2b). The dip of F1, limited by the static footwall block, remained invariable throughout the experiment (Fig. 2b). All models underwent 10 cm of total extension (Table 2), and syn-kinematic

https://doi.org/10.5194/egusphere-2022-1183
Preprint. Discussion started: 12 December 2022

sedimentation was added systematically every 5mm of extension keeping the pre-extensional regional datum constant (top of pre-kinematic unit above the static block). The newly developed basins were filled by alternating red, white, and black syn-kinematic sand layers and the positive reliefs caused by salt inflation were episodically eroded (Fig. 2b). The extensional procedure was systematically repeated for models DOM9, DOM12, DOM19, and DOM21, but they were subsequently shortened 10 cm to reach total inversion (Fig. 2c and Table 1). During this stage, no syn-kinematic sedimentation was applied nor erosion and therefore, the top of the model corresponded to the inverted geometry of the extensional basins. This procedure was applied to not distort the inversion of the faults and the contractional reactivation of salt structures by the syn-kinematic sedimentation.

At the end of the experiments, both pairs of extension-inversion models were covered with sand preserving the final topography but also preventing polymer flow. Finally, they were preserved with a gelling agent and sliced perpendicular to the trend of the major structures in closely spaced vertical serial sections (3mm-thick) with a slicing machine.

11.1.2 Mechanical properties of the analogue materials and scaling

Analogue materials consisted of layered moderately well-rounded colored and uncolored dry quartz sand simulating the brittle behavior of the upper crust rocks (Davy and Cobbold, 1991; Lohrmann et al., 2003), and a silicone polymer (polydimethylsiloxane or PDMS) that deformed as a viscous flow simulating salt in nature (Weijermars, 1986; Weijermars et al., 1993; Couzens-Schultz et al., 2003; Dell'Ertole and Schellart, 2013). The silica sand, with Mohr-Coulomb rheology (Horsfield, 1977), was sieved to homogenize the grain sizes averaging 65 to 125 µm. to color it, dyes were used without any appreciable disturbance in the mechanical properties. The sand has a bulk density of 1500 kg.m^{-3}, an angle of internal friction between 30-35º, a coefficient of internal friction of 0.59, and a low apparent cohesive strength of 78-142 Pa (Jagger and McClay, 2018). The PDMS polymer used to simulate the salt has a density of 972 kg.m^{-3} and a viscosity of 1.6 x 10^{-4} Pa.s when deformed at a laboratory strain rate of 1.83 x 10^{-4} Pa.s at room temperature thus having a near-perfect Newtonian behavior (Ferrer et al., 2017). Finally, the methodology by Hubbert (1937), Davy and Cobbold (1988), and Schellart (2000) has been used to dynamically scale the models with natural analogues by a factor of 10^{-5} (Table 2).

[Table 2]

1.1.3 Data capture, analysis, and visualization techniques

~~Classical analogue modelling workflow was followed in this study (Fig. 3).~~ Time-lapse photography, with images taken every 2 minutes with high-resolution cameras, was used to record the evolution of the models both, from the laterals as well as from the top of the model. Once the models were finished, they were closely sliced, and the resultant vertical slices were photographed with high-resolution cameras. Photographs of the final vertical slices were used to create 3D voxels that allow to be virtually sliced in any direction (see Dooley et al., 2009; Ferrer et al., 2016 and 2022a for more details). The workflow proposed by Hammerstein et al. (2014) has been improved in-house converting the final serial sections into synthetic seismic,

https://doi.org/10.5194/egusphere-2022-1183
Preprint. Discussion started: 12 December 2022

allowing them to be imported into commercial software (Ferrer et al., 2022b). The resultant input data is a 3D SEG-Y of each model that is then used to perform the interpretation of the different faults and horizons. Since the data is then possible to be visualised in 3D, the interpretation is better constrained in all directions thus reducing the uncertainties (Fig. 3). Once the interpretation is finished, the different elements can be gridded and trimmed against cutting elements and obtaining a final 3D structural model of each experiment. This workflow allows to use all the software capabilities (i.e., visualisation, interpretation, and surface modelling) to then obtain high-resolution surfaces that are well-constrained, and therefore, interpolation issues, as well as oblique geometries are minimised (Fig. 3).

[Figure 3]

1.2 Experimental results

This section presents the results of the four pairs of extension-inversion models that integrate the systematic experimental program (Table 1). Models DOM4, DOM5, DOM6, and DOM8 analyse the interplay between the thickness of the pre-extensional polymer layer and the overburden above a planar-rotational basement fault system whereas, DOM12, DOM19, DOM9, and DOM21 focus on the inversion of these extensional models (Table 1). To make it clearer, this chapter has been divided into two sections where the initial one summarizes the results of the extensional models (see Ferrer et al., 2022a) for a more detailed description of models DOM4, DOM5, DOM6, and DOM8), and the second section reports the evolution of extensional models during subsequent inversion.

1.2.1 Extensional episode

The results from the extensional models show that, in general, there is a similar pattern in the development of structures and geometries affecting the overburden (Fig. 4) but with significant differences depending on the interaction between polymer and overburden thicknesses. Subsalt extensional half-grabens with antithetic faults are the most prominent structures accommodating extension in the sand unit as the basement blocks rotate. Salt migration occurs in all models thus conditioning on the one hand the coupling between basement/overburden and the development of primary welds that compartmentalize the salt layer; and on the other hand, the development of salt-related structures. Syn-extensional sand layers are mostly deposited in salt-detached ramp syncline basins (*sensum* Roma et al., 2018b and c) that grow at the hanging wall of each fault block (Fig. 4). The architecture of the basins changes abruptly once the pre-salt impinges the overburden at the footwall of basement faults. This triggers the development of salt-detached structures at the upper hinge of the monoclines controlling the location of the depocenters (Ferrer et al., 2022a) (Fig. 4). Finally, it should be noted that the apparatus design forces a differential displacement of the fault blocks, decreasing progressively from fault F4 towards fault F1 (Fig. 2a). Consequently, the structures located closer to the moving wall will be more evolved compared to the ones of the fixed wall (Fig. 2b).

[Figure 4]

https://doi.org/10.5194/egusphere-2022-1183
Preprint. Discussion started: 12 December 2022

Model DOM4 with a thin polymer and a thick pre-kinematic overburden is characterised by the development of drape fold monoclines above the major basement faults during early extension. As the extension progresses, the monoclines are breached, eroded, and the basinward panel rotates clockwise attaining a steeply dipping attitude (F3 and F4 in Fig. 4a). The salt layer partitions the deformation below and above it, and therefore, salt-detached structures developed at different structural positions to accommodate extension. Salt migration favours the development of salt-cored anticlines slightly offset of the basement faults at the upper hinge of the monoclines. Basement impinging on the pre-kinematic overburden triggers the development of crestal collapse grabens at the crest of the salt-cored anticlines by thin-skinned extension (F2 in Fig. 4a). As deformation progresses, basement faults cut through the complete sedimentary succession and crop out favouring the breaching of the basinward monocline developed at the early stages of deformation (F3 and F4 in Fig. 4a). Salt welds develop in three of the four fault blocks thus recording salt migration towards the diapirs that developed at the footwall of the extensional faults. Further extension entails the fall of reactive diapirs with the development of collapse grabens that are filled with syn-extensional sediments (Fig. 4a).

Model DOM5 with a thin polymer and a thin overburden also developed drape fold monoclines dipping towards the moving wall but in this case, they are narrower and with a higher dip than in model DOM4 (compare the dips of the drape monoclines above F1 in Figs. 4a and 4b). As extension progresses, the tilt of the monoclines increases developing a forced fold and local salt inflation. Forced folds were breached and a discontinuous fault weld developed between the overburden panel of the forced fold and the extensional fault plane (Fig. 4b). As in model DOM4, salt migration developed salt-cored anticlines, but in this case, they were locally eroded. The impinging of the basement against the overburden formed salt welds that pinned the deformation above and below the decoupling layer. This triggered the growth of small crestal grabens at the thinned eroded roof of the salt-cored anticlines that rapidly evolve to thin-skinned low angle basinward-dipping listric faults (Fig. 4b). Likewise to model DOM4, primary welds developed below the synclinal basins at the hanging wall of faults F2, F3 and F4.

Model DOM6 with a thick polymer and thick overburden displayed a smooth initial topography with the development of drape monoclines above the basement faults and salt-cored anticlines slightly offset of the basement faults due to salt migration (Fig. 4c). As deformation progressed, the impinging of the basement against the overburden nucleated steeply dipping to vertical faults that breached the monoclines (Fig. 4c). As in models DOM4 and DOM5, early extension is partially accommodated by extensional grabens affecting the pre-kinematic roof of the salt-cored anticlines (F2 in Fig. 4c). Basement impinging enhanced the growth of salt-detached basinward-dipping faults affecting the grabens and isolating asymmetric triangular reactive diapirs at their footwall. The thick pre-kinematic overburden and the sedimentation rate applied to the model inhibited salt piercing and reactive diapirs that were progressively buried (see reactive diapirs above the footwall of F3 and F4 in Fig. 4c). Due to the salt/overburden thicknesses, salt welds between cover and basement do not develop below the ramp-syncline basin, and they are only localised at the basement impinging areas and at the hanging wall of the salt-detached basinward dipping fault in rotating block 3 (Fig. 4c).

Finally, model DOM8 with a thick polymer and a thin overburden displays mostly outcropping diapirs flanked by ramp syncline basins (Fig. 4e). As in the other models, a drape fold formed above the basement faults at the beginning of the extension (Fig. 4e). However, the dip of the drape fold at the end of the model is the highest of all the models (almost 80º dipping basinward at the end of the experiment) (Fig. 4e). The relationship between the salt and overburden thicknesses favours

https://doi.org/10.5194/egusphere-2022-1183
Preprint. Discussion started: 12 December 2022

a quick migration of salt during the early stages of extension and the development of wider and higher salt-cored anticlines than in any other model. This also causes the rise of the roof above the fixed regional surface, which is systematically eroded during the deposition of syn-extensional sand layers. Consequently, there is an erosional salt piercement that triggers the growth of passive diapirs. The lack of salt-detached extensional faults as extension increases is due to the widening of these diapirs accommodating extension (Fig. 4e). Salt welds between the overburden and the basement developed below the main ramp syncline syn-extensional basins were favoured by salt migration that in turn favoured the subsidence of the basin. With more extension and therefore, more salt migration, the welds widened away from the depocenter towards the edges of the fault blocks (Fig. 4e).

1.2.2 Inversion ~~episode~~

The four extensional models described in the previous section were repeated without changing any of the parameters and were ~~afterwards~~ inverted ~~changing the sense of deformation transferred of the motor-driven worm-screw to the rotating blocks~~ (Fig. 2c). At the end of compression, models were totally inverted (Bally, 1984) recovering the amount of extension. All the pre-extensional units were elevated attaining an almost horizontal attitude and at the same height as the regional (reference level that has been deformed neither under extension nor under compression which is located at the end fixed wall) at the end of the models (Fig. 5). During inversion, all the models show how inherited extensional basement faults were contractionally reactivated (F1 to F4, in Fig. 5) but also, the development of shortcuts at the footwall of basement faults (Fig. 5). Arching and uplifting of the synclinal basins were noticed in all the models, but although the amount of shortening is the same in all the models (10 cm), the evolution, structural height and geometry of the basins is clearly different (Fig. 5). As far salt structures are concerned, these models provide a set of reactivated salt structures by tectonic inversion from which their inherited extensional geometry is well known.

[Figure 5]

Model DOM12, which is the inverted equivalent to DOM4 (Table 1), displays all the salt-detached ramp-syncline basins completely inverted and even crestal collapse grabens developed during the inversion phase (Fig. 5a). Compression also caused the slight inversion of the inherited grabens and associated diapirs. All the newly developed thrusts affecting the overburden are directed towards the fixed wall of the model except for the one located closest to the fixed wall above F1 that is directed towards the mobile wall (Fig. 5a). It is interesting how fault welds inherited from the extensional stage are reactivated during the inversion and are opened. This opening occurs due to the impinging between the hanging wall of the basement shortcut and the overburden. This process can be identified by the shortened length of the welded succession between the overburden and basement above all the faults. In contrast, the location and the length of the primary welds below the ramp syncline basins barely change during the inversion (compare the welds in Figs. 4a and 5a).

Model DOM19, which is the inverted equivalent to DOM5 (Table 1), displays similar geometries as DOM12 with all the ramp-syncline basins completely inverted. Due to the inversion and uplift of such extensional basins, crestal collapse graben or extensional normal faults dipping towards the main basement fault are formed at the outer arch of the sedimentary succession

https://doi.org/10.5194/egusphere-2022-1183
Preprint. Discussion started: 12 December 2022

(Fig. 5b). Contractional deformation also produced the inversion of the low angle basinward-dipping listric faults inherited from the extensional episode. This reactivation produced either overthrusting of part of the pre-kinematic overburden or folding and uplifted of the small half-grabens at their hanging wall (F2 and F4 respectively in Fig. 5b). In contrast, the structural style of the inverted half-graben related to F3 is slightly different, and although the inherited listric fault was inverted, it was subsequently decapitated by a thrust directed towards the fixed wall (F3 in Fig. 5b). This difference on the structural style could be related to a greater impinging of the hanging wall of the basement shortcut against the overburden. Contrasting with the overburden deformation, the deformation at the basement level is mostly accommodated by the recovery of the extension at the main basement fault as well as by the development of footwall shortcuts (Fig. 5b).

Model DOM9, which is the inverted equivalent to DOM6 (Table 1), shows a quite different structural style compared to models DOM12 and DOM19. In this case, the thick salt layer and the thick overburden played a key role in the deformation of the overburden and the geometry of the salt-related structures during the inversion. The arching and uplift of the inverted basins at the end of the shortening were smaller than in the two previous models and no crestal collapse grabens developed (Fig. 5c). Contractional deformation amplified the salt-cored anticline above the F2 (Fig. 5c), but the most outstanding structures are the thrusts directed towards the fixed wall that nucleated at the apex of the reactive diapirs and override the syn-extensional sequences of the footwall (F3 and F4 in Fig. 5c). The evolution of this process was the compressional reactivation of the former extensional fault that, due to the overburden thickness, it inhibited the total inversion and as compression continued, a newly generated thrust broke through the extensional fault leaving part of it at the hanging wall of the thrust (Fig. 5c). In addition, the clockwise rotation of the basement blocks during inversion caused a redistribution of the primary welds below the different ramp-syncline basins and the reopening of the fault welds developed by basement impinging above the main faults during the extensional episode (compare the location of primary welds in Figs. 4c and 5c).

Finally, model DOM21, which is the inverted equivalent to DOM8 (Table 1), is the only experiment in which salt is cropping out at the end of the inversion forming contractional salt sheets (Fig. 5d). Salt migration had an important role in this model as evidenced by the fact that the inherited salt-detached ramp-syncline basins with onlaps at both limbs (Fig. 4d) are displayed as turtle structures at the end of the inversion (basins above F1 and F2 in Fig. 5d). The clockwise rotation of the basement blocks during inversion reopened the fault welds above major basement faults allowing salt migration towards the diapirs as the inherited primary welds below the basins widened (compare the location and extension of primary welds in Figs. 4d and 5d). The extrusion rate allowed the preservation of a pre-kinematic shoulder next to the diapir above F2 (Fig. 5d). In contrast, the thick hanging wall of the faults developed by basement impinging during the extensional episode in faults F3 and F4 (Fig. 4d) collapsed and sunk into the salt (Fig. 5d). While some of these collapsed blocks become welded after sinking (F4 in Fig. 5d), others rotated counter-clockwise expulsing salt probably during and after sinking (F3 in Fig. 5d).

1.3 Discussion

This section covers three main topics of interest when working with basins that underwent inversion with a pre-extensional salt layer thick enough to decouple deformation above and below it. Several questions have risen after performing the experiments and evaluating the results. Among others, the most important are: a) how does the style of salt-related structures

https://doi.org/10.5194/egusphere-2022-1183
Preprint. Discussion started: 12 December 2022

change during inversion?; b) How does the basement configuration under extension conditions the distribution of syn-tectonic sediments? and; c) How inversion tectonics impacted the salt migration, primary welds, and the final geometry of the inverted basin?.

1.3.1 How does the style of salt-related structures changes during inversion?

Salt distribution is a key aspect that should be considered when interpreting the evolution of a basin. Even more, if the basin is affected by several stages of deformation since the initial salt distribution would be difficult to reconstruct if it migrated through time and the lack of syn-deformation sequences occurs (Yin and Groshong, 2006; Rowan and Ratliff, 2012). The advantage of analogue modelling is the possibility to understand processes and geometries that might occur or develop in nature and therefore, knowing how salt migrated through the evolution of the model will help understand the location of basins or newly developed faults. In the present experimental program, salt migration occurred during the extensional phase, with salt accumulations towards both, the hanging wall and footwall of the basement extensional faults (see Fig. 3 by Ferrer et al., 2022a). The counter-clockwise rotation of the basement blocks triggered salt migration that in turn, it is controlling the development of salt-detached ramp-syncline basins, the ~~impinging of the basement against the overburden,~~ the development of primary and fault welds, the development of salt-detached extensional faults, and the rise and fall of diapirs (Fig. 4 and Fig. 6 a to d). These processes are discussed in depth by Ferrer et al. (2022a), and for such reason, they are not going to be described in detail in this section. Nevertheless, a highlight of the most important points is given so to then understand how the inherited extensional configuration conditions the evolution during tectonic inversion.

[Figure 6]

The pre-extension configuration of the model was characterised by salt being flat layered and isopach throughout the model. At the beginning of the extension, salt was stretched and migrated towards the footwall and, especially, the hanging wall of the main basement faults (Fig. 4). Sinking of ramp-syncline basins pushed away the underlaying salt by hydraulic-head gradient (Hudec and Jackson, 2007), and finally touched down the top of the basement forming a primary weld that can enlarge as extension increases and salt was expulsed (Fig. 4). In addition, drape monoclines develop above each basement fault, and if extension progresses, the basement impingement against the overburden forces the breaching of these monoclines by faulting (Fig. 4). Relict salt can be trapped at the footwall of antithetic faults along the basement fault plane forming discontinuous welds (Fig. 4a and b) (Rowan et al., 2012). Salt is also expulsed downward as the syncline-basins drag onto the basement fault forming a composite fault-fault weld surface (Stewart, 2014). If the extension continues, significant shear can be involved along these surfaces.

The inherited structural grain as well as the continuity of the salt layer or its welded equivalent at end of the extension highly condition the processes and structures developed during a late shortening event (i.e., inversion). Salt thickness, as has been previously described during extension, controls coupling/decoupling between basement and overburden during the contractional deformation (Letouzey et al., 1995). Under compression pre-existing diapirs (i.e., passive diapirs in model DOM8, Fig. 4d), as the weakest part of the models, are squeezed earlier increasing the salt-rise rate. This fact, together with

https://doi.org/10.5194/egusphere-2022-1183
Preprint. Discussion started: 12 December 2022

not considering syn-inversion sedimentation, allows the emplacement of allochthonous salt sheets in an extrusive advance mode (Hudec and Jackson, 2006) (Fig. 5d). During inversion, buried diapirs were rejuvenated, and or the inherited salt-detached extensional faults above them were inverted (white faults in models DOM12 and DOM19, Fig. 5a and b), or newly formed thrusts nucleating at the apex of the reactive diapirs developed (yellow faults of the overburden in model DOM9, Fig. 5d) (Roma et al., 2008a). In addition, the thickness of the cover sequence above salt accumulations (salt-cored anticlines) conditioned the locus of thrusts during inversion favouring the development of thrusts if the cover was either already thin or thinned by local erosion during extension (hinterland-directed thrust above F2 in Fig. 5b compared to Fig, 4c, and Fig. 6f). In contrast, a thick pre-extensional overburden (salt-cored anticlines above F2 in Fig. 4c) will confine the salt during the compression and salt accumulations will be accentuated (equivalent structures in Fig. 5c and 6g). On the other hand, regional shortening forced the clockwise rotation of the basement blocks (thick-skinned deformation) having a critical impact on the inherited weld distribution that was strongly modified (Fig. 6). Depending on the structural position, welds can be enlarged if they were developed in the central part of basement blocks, but they can also be reopened where basement blocks impinged the overburden in models with a thick salt layer (DOM9 and DOM 21, Figs. 5c and d respectively). This process can be deduced by comparing the location of welds developed during the extensional phase that are either not present at the end of compression or that have shifted their location during the inversion phase of the model (Fig. 6 a to d against Fig. 6 e to h).

1.3.2 How does the basement configuration under extension condition the distribution of syn-tectonic sediments?

It is well established that if salt is thick enough, deformation can be decoupled above and below the salt layer but also conditioning the location of newly developed structures at the foreland (e.g., Withjack et al., 1989; Koyi et al., 1993; Jackson and Vendeville 1994; Stewart and Clark, 1999; Withjack and Callaway 2000; Alves et al., 2002; Dooley et al. 2005; Ferrer et al., 2012 and 2016; Duffy et al., 2013; Lewis et al., 2013; Warsitzka et al., 2015; Carola et al., 2017; Jackson et al., 2019; Dooley and Hudec, 2020). This process can be observed in the experiments by comparing the isobaths map of the base of salt and the thickness map of the syn-extensional successions (Fig. 7). At a first glance, it is obvious that this decoupling occurs since both, the thickness maps of the salt and the overburden are different (Figs. 6 and 7) but also by the misalignment in space of the syn-extensional depocenters and the deepest points of the downthrown basement blocks (Fig. 7). More in detail, these parameters present differences that allow to investigate even deeper the impact of salt and cover thickness into the evolution of all models as discussed below.

[Figure 7]

In the models with a thin polymer layer and a thick overburden sequence, the main extensional faults caused the downthrown of the hanging wall down to depths of more than -40 mm in areas close to the basement extensional faults (Fig. 7a). During this stage, the combination of salt migration and downthrown displacement allowed for the developed ramp-syncline basins reaching a total thickness of 36 mm. The depocenter is not located right above the basement extensional faults but close to them (Fig. 7e). In contrast, the other end member is the model with a thick polymer and thin overburden sequence which displays the same displacement for the deeper levels with more than -40 mm of throw (Fig. 7c) whereas, the thickest syn-sedimentary succession reaches between 28 mm and up to 32 mm at the thickest part (Fig. 7g). Intermediate models with a

https://doi.org/10.5194/egusphere-2022-1183
Preprint. Discussion started: 12 December 2022

thin polymer and overburden sequences display downthrown displacements of up to -40 mm (Fig. 7b) and syn-extensional successions up to 36 mm to 40 mm (Fig. 7f) thus behaving as a more coupled deformation and therefore, the influence of salt in these cases is less important.

All the described extensional geometries can be attributed to the decoupling level that provides the polymer by simply comparing these geometries with the ones developed under the same parameters but with models lacking the polymer such as the ones performed by Buchanan and McClay (1992) and by Jagger and McClay (2018). The results from the models of the previous authors under extension show how the location of the main depocenters is immediately above the basement extensional faults and with a trajectory that is parallel to the main fault (Fig. 2a of Buchanan and McClay, 1992 or Fig. 4a of Jagger and McClay, 2018). In contrast, the models reported by Ferrer et al. (2022a) and here, show how the location of the depocenters is highly conditioned by the thickness ratio of salt *vs* overburden and that they are not located immediately above the main extensional faults. In addition, through time, the trajectory of the salt-detached ramp-syncline depocenters is not lineal but curved thus recording the salt migration process that occurs as extension progresses (Fig. 4).

1.3.3 How does inversion affects salt migration, primary welds, and the final geometry of the inverted basin?

The compressional geometries and newly developed structures are highly influenced by the decoupling layer. When comparing these geometries with the ones developed with similar experimental apparatus and setups without mechanical anisotropies performed by Buchanan and McClay (1992) and by Jagger and McClay (2018), stands out that the polymer acts as a mechanical discontinuity and impacts on the development of inversion structures. Their results show how the structures accommodating deformation during the inversion are basement extensional faults reactivated as reverse faults and shortcuts developed at their footwalls (Figs. 2 to 6 of Buchanan and McClay, 1992 or Figs. 4 to 9 of Jagger and McClay, 2018). In contrast, in the models here presented, the contractional reactivation of basement structures and shortcuts occurs (F1 to F4 white basement faults in Fig. 5), but the deformation is effectively decoupled by the polymer layer. In this sense, the main contractional structures are salt-detached foreland- and hinterland-directed thrusts (yellow faults affecting the overburden in Fig. 5c and Fig. 5b respectively), compressionally amplified salt-cored anticlines (Fig. 5c), and salt sheets (Fig. 5d). The decoupling layer also impacts on the structural relief developed during the inversion (Fig. 8). A correlation between polymer thickness and overburden structural relief has been observed in the experiments, independently of the pre-kinematic overburden thickness, where the thinner the polymer the higher the structural relief (Fig. 8). Therefore, the role that the salt layer plays in the development of structures allowing to generate relief is directly related to the degree of decoupling between sub- and supra-salt units. As pointed out before, depending on the ratio between polymer and overburden thicknesses, some structures might develop more predominantly than others and consequently, in natural cases, the thickness of the decoupling layer must be considered when interpreting the actual geometry of inverted basins, when deriving the evolution of a basin or how it evolved during inversion.

[Figure 8]

https://doi.org/10.5194/egusphere-2022-1183
Preprint. Discussion started: 12 December 2022

One of the processes observed during inversion was the reopening of inherited primary welds. Reopening of salt-depleted mechanical contacts is well observable when comparing salt thicknesses at the end of the extensional and the compressional stages (Fig. 9). Mapping the location of welded areas both, after extension and after inversion, shows that their location is not perfectly aligned or even some welds developed under extension not being present at the end of inversion (Fig. 9a). For simplicity, the location of welds at the end of extension has been split into two different groups in this figure. The first group are welds developed below the salt-detached ramp-syncline basins (Fig. 9b) whereas the second group are welds developed immediately next to a basement fault (Fig. 9c). The first group of welds develops when the sinking ramp-syncline basins touch down to the basement during basement extension and widen updip (Fig. 9b). As extension progresses, basinward salt-detached extensional faults are triggered by the impinging of basement blocks against the overburden (Ferrer et al., 2022a). This results in a characteristic geometry where the weld is flanked by two salt accumulations bounded by faults, one at the hanging wall of the basement fault and the other at the footwall of basinward-dipping salt-detached extensional fault (reactive diapir in Fig. 9 a and b). During the inversion, the clockwise rotation of the basement blocks forces the reopening of inherited primary welds from the hinterland towards the foreland as seen by the shift in welds location between extension and inversion stages (Fig. 9 a and b). This process is common in models where decoupling is more accentuated and therefore, models with thicker polymer successions are more prone to reactivate this type of welds under compression (DOM9 of Fig. 5). The second group of welds is characterised by two salt accumulations separated by a weld developed due to the basement impinging against the overburden during the extensional movement and the counter-clockwise rotation of basement blocks (Fig. 9c). The local weld formed by basement impinging can increase in length as basement extension progresses. Salt is gradually expelled downward as the overburden rolls onto the basement fault plane enhanced by the counter-clockwise rotation of basement blocks. As Steward (2014) proposed, the coupling between the basement and the overburden also allows the reactivation of the weld developed above the basement fault as a fault weld with increasing extension (Fig. 4).

[Figure 9]

The reopening of extensional fault welds is a continuous process that involves the inversion of the former extensional basement fault as well as block rotation above and below the salt (Fig. 10). The pre-inversion configuration is characterised by a fault weld as well as weld below the ramp-syncline basins that puts in contact the succession above and below the decoupling layer (Fig. 10a). Once compression initiates, inversion of the basement fault starts to uplift the whole hanging wall succession and rotation of the basement block occurs. At this mild inversion stage, both welds are still closed, and inversion is evidenced by the development of a foreland-directed thrust generating some structural relief that is going to be active up to the end of compression (Fig. 10b). As inversion progresses, the fault weld is totally reactivated and reopens thus connecting the two salt accumulations developed during the extensional stage and allowing the salt to passively flow between the two accumulations (Fig. 10c). This explains why some of the welded areas under extension are not present at the end of the inversion as shown in figure 9a. In addition, this salt migration causes the counter-clockwise rotation of the ramp-syncline basin causing the initiation of the reopening of the weld developed below the basin, and therefore, salt migrates towards the newly generated space (Fig. 10b). During this stage, sub-salt compression is partially absorbed by the reverse movement of the former basement extensional fault but also by the generation of footwall shortcuts. Finally, total inversion is characterised by the almost horizontal disposition of sub-salt strata, the total reopening of the fault weld and an active process of weld reopening and salt migration as the ramp-syncline basin continues to rotate (Fig. 10d).

Experiments have shown that this process is more accentuated in models with a thicker polymer layer since decoupling is also more accentuated while in models with a thin polymer layer, reopening hardly occurs as shown by the preservation of the basement impingement at the end of compression which was developed at the footwall of the master faults during extension (Fig. 5 a and b and Fig. 6 e and f). It is important to remark that in the models, as in nature, it is not the salt that reopens the welds, but rather the basement blocks involved in the compressional deformation that does the active work (thick-skinned deformation). The role of salt is passive and twofold: 1) it flows and occupies the space generated during the rotation of blocks, and 2) it acts as a decoupling layer allowing the overlying basins to accommodate the thick-skinned deformation. It is also worth mentioning that the confinement of the salt coupled with the non-existence of inherited salt structures (i.e., diapirs and walls) could play a major role in conditioning weld reopening. A well-developed network of diapirs, inherited from the extensional episode, could inhibit the reopening of welds since they would be preferentially squeezed at the onset of the contractional deformation developing salt sheets (Dooley et al., 2009; Santolaria et al., 2021). Once most of these diapirs were secondarily squeezed and depending on the volume of preserved salt in the source layer, the primary welds could be reopened. This is a factor that has not been tested in the current research and it is worth to consider in future models.

[Figure 10]

Although the experimental outcome presented here shows how two different types of primary welds (i.e., welds below salt-detached ramp-syncline basins and welds developed above basement faults) inherited from an extensional episode reopened during subsequent thick-skinned contractional deformation, to our knowledge, the process that leads to the welds reopening has not been described in the literature. The closest process for explaining weld reopening below the salt-detached ramp-syncline basins would correspond to salt delamination of deep salt wings described in the Northwest German and Polish basins (Baldschuhn et al., 2001; Rowan and Krzywiec, 2014). According to Hudec (2004), in that case, the Late Cretaceous regional shortening produced the injection/intrusion of the deeper Permian Zechstein and Rotliegend salt into shallower Triassic Röt salt forming wings on the flanks of many salt diapirs of the area. Rowan and Krzywiec (2014) point out that contractional deformation was not injected salt into the wings, and that the process must be viewed as a passive flow into the space created during folding and uplift of the flanking strata adjacent to the diapirs during the squeezing of buried diapirs by regional shortening. Dooley et al. (2009) described a similar process in analogue models simulating deeply buried diapirs that were subsequently contractionally rejuvenated. According to this work, the salt from a diapir can flow back into the source layer during the squeezing of a deeply buried diapir defining an outward intrusive plume of salt that injects towards the foreland and uplifts the overburden. In our opinion, in this case, the use of the term injection would not be appropriate since salt is only passively flowing towards the new space created by cover uplift during regional shortening. In the models presented here, the welds below the ramp-syncline basins are reopened due to the rotation of basement blocks, which are decoupled from the cover by the salt layer, they delaminate generating new space that is passively occupied by salt. Similarly, in the welds that reopened above basement faults (Fig. 11), the active mechanism is the thick-skinned inversion that caused the inversion of the fault and the uplift/rotation of the adjacent basement blocks. Nevertheless, in this case, the two isolated salt volumes by a

https://doi.org/10.5194/egusphere-2022-1183
Preprint. Discussion started: 12 December 2022

primary weld formed by the basement impinging against the overburden at the end of the extension (Fig. 4c and d), are connected allowing the salt to passively flow between these two areas (Fig. 5c and d). The reopening of those welds is not suitable for the delamination process since the control of the vertical movements of the basement blocks during inversion is critical for reopening. It should be noted that thick-skinned contractional deformation during inversion is the motor that controls weld reopening and that the salt merely flows into the newly created spaces. This process has never been described in the literature, neither in real cases nor in analogue or numerical models, and therefore, this research provides new insights on weld reactivation and salt tectonics which should be considered in the future.

Finally, of interest is the geometry of the ramp-syncline basins at the end of the compressional stage and how it relates to the initial thickness of salt. In all the cases with a thin polymer succession, a total inversion of the basin is observable (Fig. 5 a and b), whereas in models with a thick polymer, the resultant geometry of the ramp-syncline basins does not show a total basin inversion rather, no inversion at all or a partial inversion is documented (Fig. 5 c and d). In the models with a thick polymer and a thick overburden, the hinterland basins are slightly rotated and thrust over the more external basins while the basins located in a more foreland position preserved the extensional geometry. In these models, deformation is absorbed by the salt migration into thickened salt-cored anticlines and uplifting of the overburden (Fig. 5c). The preservation of the extensional geometries pre-dating the development of fold-and-thrust belts is rather common as reported in several basins that underwent partial inversion and orogens around the world such as the Apennines, the Pyrenees or the Betics (Scisciani et al., 2014; Carola et al., 2015; Saura et al., 2015; Escosa et al., 2018). On the other hand, models with a thick polymer and a thin overburden sequence are characterised by geometries grown during the inversion stage related to salt migration processes which developed turtle structures but also the generation of salt sheets or salt glaciers (Fig. 5d). Similar processes have been described in Gabon, Morocco, the sub-Alpine fold-and-thrust belt where compressional salt glaciers are developed during the growth of the orogen (Ventisette et al., 2005; Hudec and Jackson, 2006; Jackson et al., 2008; Graham et al., 2012; Fernández et al., 2020; Flinch and Soto, 2022).

In summary, the results shown in this research provide a useful tool when working in areas that underwent inversion of an extensional system with a pre-extensional decoupling layer. The resultant geometries can be categorised depending on the different thicknesses of both, the salt and the pre-extensional cover successions (Fig. 11). While a thin salt and thin pre-extensional cover results in a more coupled deformational style both during extension and inversion, the opposite occurs when the salt and the pre-extensional successions are thick and therefore, a completely decoupled deformation is observed. In the former case, the geometries after extension are characterised by a short and steeply dipping monocline which develops a long fault-weld with impingement of the basement and above the monocline, an extensional basin located close to the basement extensional fault. The geometries after total inversion are characterised by the preservation of the basement impingement and by the total inversion of the syn-extensional succession with collapse faults affecting this succession. In the latter case, the geometries which characterise the models after extension are different depending on the thickness of the pre-extensional overburden. If it is thin, passive diapirs develop by erosion of a salt-inflated area and therefore most of the extension is accommodated within these structures. In contrast, a thick cover results in the development of reactive diapirs that with the syn-extensional sedimentation rate applied in the experiments ended up as buried salt accumulations. Although the geometries and processes are different, in both cases there is the development of a large monocline, the growth of an extensional basin above the monocline whose depocenter is not located close to the main basement fault and a less important basement

https://doi.org/10.5194/egusphere-2022-1183
Preprint. Discussion started: 12 December 2022

impingement compared to the previous case. The geometries after total inversion are also different depending on the cover thickness and for a reduced cover, the most common geometry is the preservation of some of the outcropping salt structures and the development of salt sheets whereas, with a thick cover, the reopening of welds and the development of foreland-directed thrusts are the most important structures absorbing shortening.

[Figure 11]

1.4 Conclusions

Geometries and evolution of inversion tectonics of domino extensional basement-fault systems have been previously investigated by some authors using analogue models but without testing the role of a mechanical discontinuity such as a salt layer and consequently, the influence of a decoupling layer has never been performed before. This study focussed on revealing the implications accounted during the inversion of extensional basement-fault half-grabens with a pre-extensional intermediate decoupling layer by means of analogue modelling.

One of the main results shows that the ratio between polymer and overburden thicknesses highly conditioned the evolution of the former extensional basins under compression. The amount of overburden structural relief developed during the inversion is directly related to the thickness of both, the syn-extensional deposition as well as the polymer layer. From the experimental program it is proposed that the thicker the polymer and overburden successions, the smallest the overburden structural relief. In contrast, when the polymer layer and the overburden are the thinnest, the resultant overburden structural relief is the highest. This is related to the coupling of the deformation between the successions above and below the polymer layer and therefore, when the two successions are completely coupled, the inversion of basement faults uplifts the overburden succession thus increasing the overburden structural relief.

Another main result from the study is the characterisation of inherited weld reopening during the compressional episode. ~~Even that~~ weld reopening under ~~compression~~ occurs to a greater or less extent in all models, welds developed in models with the thickest polymer and syn-extensional successions are the most likely to be reactivated. During extension, welds were developed either below the salt-detached ramp-syncline basins or immediately above the basement faults. In the former case, the weld developed during extension by salt migrating towards the adjacent hanging wall and footwall of basement faults. During the compressional episode, the weld is partially reactivated reopening the hinterland part of the weld and at the same time, the weld is enlarged towards the foreland. In the latter case, the extensional weld was generated due to salt migration as well as sagging of the overburden until the succession was impinged by the basement. During inversion, the weld reopens thus connecting the two salt accumulations and allowing the salt to passively migrate between the two and resulting in that at the end of the compression there is not a record of the presence of this extensional weld.

Finally, the study shows that the way the ramp-syncline developed under extension, is inverted in the compressional stage is highly conditioned by the salt thickness and therefore by the degree of coupling between the deeper and shallower structural levels. In that sense, the models which were characterised by a thin polymer succession resulted in a total inversion of the ramp-syncline basins while models with a thick polymer succession the inversion is barely recorded with only a small rotation of the basins or even completely preserving the extensional geometries.

Acknowledgments

This work has been partly supported by the SABREM (PID2020-117598GB-I00) and by the GEODIGIT (TED2021-130602B-I00) research projects funded by MCIN/AEI/10.13039/501100011033 and for the European Union "NextGenerationEU"/PRTR, and by the STAR Research Consortium (supported by BG Group, BHPBilliton, ConocoPhillips, ENI, MarathonOil, Nexen, Shell, Talisman Energy and YPF). The GEOMODELS Research Institute and the Grup de Geodinàmica i Anàlisi de Conques (2017SGR-596) are also acknowledged for their financial support. ~~Of~~ gratefully acknowledge Kevin D'Souza, Jerry Morris and Frank Lehane for logistical support in the modelling laboratory. We thank M.G. Rowan, B. C. Vendeville and S. Stewart for helpful discussions and suggestions. Schlumberger and Eliis are also acknowledged for providing Petrel and PaleoScan software respectively.

References

Alves, T. M., Gawthorpe, R. L., Hunt, D. W., and Monteiro, J. H.: Jurassic tectono-sedimentary evolution of the Northern Lusitanian Basin (offshore Portugal), Mar Petrol Geol, 19, 727-754, https://doi.org/10.1016/S0264-8172(02)00036-3, 2002.

Badley, M.E., Orice, J.D., Backshall, L.C.: Inversion, reactivated faults and related structures: seismic examples from the southern North Sea, edited by: Cooper, M.A., Williams, G.D., Inversion Tectonics, Geol Soc Spec Publ, 44, 201-219, https://doi.org/10.1144/GSL.SP.1989.044.01.12, 1989.

Baldschuhn, R., Best, G., Kockel, F.: Inversion tectonics in the north-west German basin, edited by: Spencer, A.M., Generation, accumulation, and production of Europe's hydrocarbons, European Association of Petroleum Geoscientists, Special Publication 1, 149-159, 2001.

Bally A.W.: Tectogénèse et seismique réflexion, Bulletin Société Géologique de France, XXIV(2), 279-285, https://doi.org/10.2113/gssgfbull.S7-XXVI.2.279, 1984.

Bonini, M., Sani, F., Antonielli, B.: Basin inversion and contractional reactivation of inherited normal faults: A review based on previous and new experimental models, Tectonophysics, 522-523, 55-88, https://doi.org/10.1016/j.tecto.2011.11.014, 2012.

Brun, J.P. and Fort, X.: Compressional salt tectonics (Angolan margin), Tectonophysics, 382, 129-150, https://doi.org/10.1016/j.tecto.2003.11.014, 2004.

Brun, J.P. and Nalpas, T.: Graben inversion in nature and experiments, Tectonics, 15(3), 677-687, https://doi.org/10.1029/95TC03853, 1996.

Buchanan, P., and McClay, K. R.: Experiments on basin inversion above reactivated domino faults, Mar Petrol Geol, 9, 486-500, https://doi.org/10.1016/0264-8172(92)90061-I, 1992.

Burliga, S., Koyi, H.A., Krzywiec, P.: Modelling cover deformation and decoupling during inversion, using the Mid- Polish Trough as a case study, J Struct Geo, 42, 62-73, https://doi.org/10.1016/j.jsg.2012.06.013, 2012.

Callot, J.P., Jahani, S., Letouzey, J.: The role of pre-existing diapirs in fold and thrust belt development, edited by: Lacombe, O., Lavé, J., Vergés, J., Roure, F., Thrust belts and foreland basins: From fold kinematic to hydrocarbon systems. 309-325, DOI: 10.1007/978-3-540-69426-7_16, 2007.

Carola, E., Muñoz, J. A., and Roca, E.: The transition from thick-skinned to thin-skinned tectonics in the Basque-Cantabrian Pyrenees: The Burgalesa Platform and surroundings, Int J Earth Sci, 104, 2215-2239, https://doi.org/10.1007/s00531-015-1177-z, 2015.

Carola, E., Ferrer, O., Vidal-Royo, O., Muñoz, J.A.: Interpretation of salt-cored frontal structures in the Southern Pyrenees guided by analog modeling, surface and subsurface data, Interpretation, 5(1), 39-54, https://doi.org/10.1190/INT-2016-0093.1, 2017.

Cartwright, J.A., Jackson, M.P.A., Dooley, T., Higgins, S.: Strain partitioning in gravity-driven shortening of a thick, multi-layered evaporite sequence, edited by: Alsop, G. I., Archer, S. G., Hartley, A. J., Grant, N. T. and Hodgkinson, R., Salt Tectonics, Sediments and Prospectivity, Geol Soc Spec Publ, 363, 449-470, https://doi.org/10.1144/SP363.21, 2012.

Coleman, A. J., Duffy, O. B., Jackson, C. A.-L.: Growth folds above propagating normal faults: Earth-Science Reviews, 196, 102885, https://doi.org/10.1016/j.earscirev.2019.102885, 2019.

Costa, E. and Vendeville, B.C.: Experimental insights on the geometry and kinematics of fold-and-thrust belts above weak, viscous evaporitic décollement, J Struct Geo, 24, 1729-1739, https://doi.org/10.1016/S0191-8141(01)00169-9, 2002.

Couzens-Schultz, B. A., Vendeville, B. C., and Wiltschko, D. V.: Duplex style and triangle zone formation: insights from physical modelling, J Struct Geo, 25, 1623-1644, https://doi.org/10.1016/S0191-8141(03)00004-X, 2003.

Davy, P., and Cobbold, P. R.: Indentation tectonics in nature and experiment. 1. Experiments scaled for gravity, Bulletin of the Geological Institutions of Uppsala, N.S., 14, 129-141, 1988.

Davy, P., Cobbold, P.R.: Experiments on shortening of a 4-layer model of the continental lithosphere, Tectonophysics, v. Tectonophysics, 188, l-25, https://doi.org/10.1016/0040-1951(91)90311-F, 1991.

Dell'Ertole, D., and Schellart, W. P.: The development of sheath folds in viscously stratified materials in simple shear conditions: an analogue approach, J Struct Geo, 56, 129-141, https://doi.org/10.1016/j.jsg.2013.09.002, 2013.

Dooley, T. P., Jackson, M. P. A., and Hudec, M.R.: Inflation and deflation of deeply buried salt stocks during lateral shortening, J Struct Geo, 31, 582-600, https://doi.org/10.1016/j.jsg.2009.03.013, 2009.

Dooley, T. P., Jackson, M. P. A., and Hudec, M.R.: Breakout of squeezed stocks: dispersal of roof fragments, source of extrusive salt and interaction with regional thrust faults, Basin Res, 26, 1-23, https://doi.org/10.1111/bre.12056, 2014.

Dooley, T.P., McClay, K.R., Hempton, M., and Smit, D.: Salt tectonics above complex basement extensional fault systems: Results from analogue modelling, edited by: Dore, A. G., and Vining, B.A., Petroleum geology: North-west Europe and global perspectives – Proceedings of the 6th Petroleum Geology Conference, London, Petroleum Geology Conferences Ltd. and the Geological Society, 1631-1648, https://doi.org/10.1144/006163, 2005.

Dooley, T.P. and Hudec, M.R.: The effects of base-salt relief on salt flow and suprasalt deformation patterns - Part 2: Application to the eastern Gulf of Mexico, Interpretation, 5, SD25-SD38, https://doi.org/10.1190/INT-2016-0088.1, 2016.

Dooley, T.P. and Hudec, M.R.: Extension and inversion of salt-bearing rift systems, Solid Earth, 11, 1187-1204, https://doi.org/10.5194/se-11-1187-2020, 2020.

Duffy, O.B., Gawthorpe, R.L., Docherty, M., and Brocklehurst, S.H.: Mobile evaporite controls on the structural style and evolution of rift basins: Danish Central Graben, North Sea, Basin Res, 25, 3, 310-330, https://doi.org/10.1111/bre.12000, 2013.

Escosa, F.O., Roca, E., Ferrer, O.: Testing thin-skinned inversion of a prerift salt-bearing passive margin (Eastern Prebetic Zone, SE Iberia), J Struct Geo, 109, 55-73, https://doi.org/10.1016/j.jsg.2018.01.004, 2018.

Fernández, O., Habermüller, M., Grasemann, B.: Hooked on salt: Rethinking Alpine tectonics in Hallstatt (Eastern Alps, Austria), Geology 49, 325-329, https://doi.org/10.1130/G47981.1, 2020.

Ferrer, O., Jackson, M.P.A., Roca, E., and Rubinat, M.: Evolution of salt structures during extension and inversion of the Offshore Parentis Basin (Eastern Bay of Biscay), edited by: Alsop, G.I., Archer, S.G., Hartley, A.J., Grant, N.T., and Hodgkinson, R., Salt tectonics, sediments and prospectivity, Geo Soc Spec Publ, 363, 361-380, https://doi.org/10.1144/SP363.16, 2012.

Ferrer, O., Roca, E., Vendeville, B. C.: The role of salt layers in the hangingwall deformation of kinked-planar extensional faults: Insights from 3D analogue models and comparison with the Parentis Basin: Tectonophysics, 636, 338-350, https://doi.org/10.1016/j.tecto.2014.09.013, 2014.

Ferrer, O., McClay, K.R., and Sellier, N.: Influence of fault geometries and mechanical anisotropies on the growth and inversion of hangingwall synclinal basins: Insights from sandbox models and natural examples, edited by: Childs, C., Holdsworth, R.E., Jackson, C.A-L., Manzocchi, T., Walsh, J.J., and Yieldings, G., The geometry and growth of normal faults: Geol Soc Spec Publ, 439, 487-509, https://doi.org/10.1144/SP439.8, 2016.

Ferrer, O., Carola, E., McClay, K.R., Bufaliza, N.: Analog modeling of domino-style extensional basement fault systems with pre-kinematic salt, AAPG Bull, DOI: 10.1306/08072221188, 2022a.

Ferrer, O., Santolaria, P., Muñoz, J.A., Granado, P., Roca, E., Gratacós, O., Snidero, M., Analogue modeling as a tool to assist seismic structural interpretation in the Andean fold-and-thrust belt, edited by: Zamora, G. and Mora, A., Andean Structural Styles: A Seismic Atlas, Elsevier, 43-61, https://doi.org/10.1016/B978-0-323-85175-6.00003-1, 2022b.

Fiduk, C. and Rowan, M.G.: Analysis of folding and deformation within layered evaporites in Blocks BM-S-8 & -9, Santos Basin, Brazil, edited by: Alsop, G. I., Archer, S. G., Hartley, A. J., Grant, N. T. and Hodgkinson, R., Salt Tectonics, Sediments and Prospectivity, Geol Soc Spec Publ, 363, 471-487, https://doi.org/10.1144/SP363.2, 2012.

Flinch, J.F., Soto, J.I.: Structure and Alpine tectonic evolution of a salt canopy in the western Betic Cordillera (Spain), Mar Petrol Geol, 143, 105782, https://doi.org/10.1016/j.marpetgeo.2022.105782, 2022.

Gowers, M., Holtar, E., Swensson, E.: The structure of the Norwegian Central Trough (Central Graben area). Geological Society, London, Petroleum Geology Conference series, 4, 1245-1254, https://doi.org/10.1144/0041245, 1993. Graham, R., Jackson, M., Plicher, R., Kilsdonk, B.: Allochthonous salt in the sub-Alpine fold–thrust belt of Haute Provence, France, edited by: Alsop, G. I., Archer, S. G., Hartley, A. J., Grant, N. T. and Hodgkinson, R., Salt Tectonics, Sediments and Prospectivity, Geol Soc Spec Publ, 363, 595-615, https://doi.org/10.1144/SP363.30, 2012.

Granado, P., Ruh, J.B., Santolaria, P., Strauss, P., Muñoz, J.A., Stretching and contraction of extensional basins with pre-rift salt: A numerical modeling approach, Front Earth Sci, 9, 648937, doi: 10.3389/feart.2021.648937, 2021.

Hammerstein, J., Truelove, L., and McClay, K. R.: Additional methods for the analysis of seismic data and risk reduction through the interpretation and reservoir modelling of scaled analogue models: https://www.searchanddiscovery.com/abstracts/html/2014/90189ace/abstracts/1841538.html (accessed July 11, 2022), 2014.

Hansen, T.H., Røno, O., Andresen, K.J.: Thick- and thin-skinned basin inversion in the Danish Central Graben, North Sea – the role of deep evaporites and basement kinematics: Solid Earth, 12, 1719-1747, https://doi.org/10.5194/se-12-1719-2021, 2021.

Hubbert, M. K.: Theory of scaled models as applied to the study of geological structures, Geol Soc Am Bull, 48, 1459-1520, https://doi.org/10.1130/GSAB-48-1459, 1937.

Hudec, M.R. and Jackson, M.P.A.: Advance of allochthonous salt sheets in passive margins and orogens, AAPG Bull, 90, 1535-1564, https://doi.org/10.1306/05080605143, 2006.

Hudec, M.R. and Jackson, M.P.A.: Terra infirma: Understanding salt tectonics, Earth Science Reviews, 82, 1-28, https://doi.org/10.1016/j.earscirev.2007.01.001, 2007.

Jackson, M.P.A., Hudec, M.R., Jannette, D.C., Kilby, R.E.: Evolution of the Cretaceous Astrid thrust belt in the ultradeep-water Lower Congo Basin, Gabon, AAPG Bull, 92, 4, 487-511, https://doi.org/10.1306/12030707074, 2008.

Jackson, M.P.A. and Vendeville, B.C.: Regional extension as a geologic trigger for diapirism, Geol Soc Am Bull, 106, 1, 57-73, https://doi.org/10.1130/0016-7606(1994)106<0057:REAAGT>2.3.CO;2, 1994.

Jackson, C.A-L., Chua, C-T., Bell, R.E., Magee, C.: Structural style and early stage growth of inversion structures: 3D seismic insights from the Egersund Basin, offshore Norway, J Struct Geo, 46, 167-185, https://doi.org/10.1016/j.jsg.2012.09.005, 2013.

Jackson, C.A-L., Elliott, G.M., Royce-Rogers, E., Gawthrope, R.L., and Aas, T.E.: Salt thickness and composition influence rift structural style, northern North Sea, offshore Norway, Basin Res, 31, 3, 514-538, https://doi.org/10.1111/bre.12332, 2019.

Jagger, L.J. and McClay, K.R.: Analogue modelling of inverted Domino-style Basement Fault Systems, Basin Res, 30, 1, 363-381, https://doi.org/10.1111/bre.12224, 2018.

Koyi, H. A., Jenyon, M. K., and Petersen, K.: The effect of basement faulting on diapirism, J Struct Geo, 16, 285-312, https://doi.org/10.1111/j.1747-5457.1993.tb00339.x, 1993.

Krantz, R. W.: Measurements of friction coefficients and cohesion for faulting and fault reactivation in laboratory models using sand and sand mixtures, Tectonophysics, 188, 203-207, https://doi.org/10.1016/0040-1951(91)90323-K, 1991.

Lacombe, O. and Bellahsen, N., Thick-skinned tectonics and basement-involved fold-thrust-belts. Insights from selected Cenozoic orogens. Geol Mag, 153, 1-48, DOI: https://doi.org/10.1017/S0016756816000078, 2016.

Letouzey, J., Colleta, B., Vially, R., Chermette, J.C.: Evolution of salt-related structures in compressional settings, edited by: Jackson, M.P.A., Roberts, D.G., and Snelson, S., Salt tectonics: a global perspective. AAPG Memoir 65, 41-60, https://doi.org/10.1306/M65604C3, 1995.

https://doi.org/10.5194/egusphere-2022-1183
Preprint. Discussion started: 12 December 2022

Lewis, M.M., Jackson, C.A.-L., and Gawthorpe, R.L.: Salt-influenced normal fault growth and forced folding: the Stavanger Fault System, North Sea, J Struct Geo, 54, 156-173, https://doi.org/10.1016/j.jsg.2013.07.015, 2013.

Lohrmann, J., Kukowski, N., Adam, J., and Oncken, O.: The impact of analogue material properties on the geometry, kinematics and dynamics of convergent sand wedges, J Struct Geo, 25, 1691-1711, https://doi.org/10.1016/S0191-8141(03)00005-1, 2003.

Nemčok, M., Gayer, R., Miliorizos, R.: Structural analysis of the inverted Bristol Channel Basin: implications for the geometry and timing of fracture porosity, edited by: Buchanan, J.G., Buchanan, P.J., Basin Inversion, Geol Soc Spec Publ, vol. 88, 355-392, https://doi.org/10.1144/GSL.SP.1995.088.01.2, 1995.

Panien, M., Screurs, G., Pfiffner, A.: Sandbox experiments on basin inversion: testing the influence of basin orientation and basin fill, J Struct Geo, 27, 433-445, https://doi.org/10.1016/j.jsg.2004.11.001, 2005.

Roma, M., Ferrer, O., McClay, K. R., Muñoz, J. A., Roca, E., Gratacós, O., and Cabello, P.: Weld kinematics of syn-rift salt during basement-involved extension and subsequent inversion: Results from analog models, Geologica Acta, 16, 4, 391-410, DOI: 10.1344/GeologicaActa2018.16.4.4, 2018a.

Roma, M., Ferrer, O. Roca, E. Pla, O. Escosa, F.O. Butillé, M.: Formation and inversion of salt-detached ramp-syncline basins. Results from analog modeling and application to the Columbrets Basin (Western Mediterranean), Tectonophysics, 745, 214-228, https://doi.org/10.1016/j.tecto.2018.08.01,22018b.

Roma, M. Vidal-Royo, O. McClay, K. Ferrer, O. Muñoz, J.A., Tectonic inversion of salt-detached ramp-syncline basins as illustrated by analog modeling and kinematic restoration, Interpretation, T127-T144, https://doi.org/10.1190/INT-2017-0073.1, 2018c.

Rowan, M.G. and Krzywiec, P.: The Szamotuly salt diapir and Mid-Polish Trough: Decoupling during both Triassic-Jurassic rifting and Alpine inversion, Interpretation, 2, SM1-SM18, https://doi.org/10.1190/INT-2014-0028.1, 2014.

Rowan, M.G., Lawton, T.F., Giles, K.A.: Anatomy of an exposed vertical salt weld flanking strata, La Popa Basin, México, edited by: Alsop, G. I., Archer, S. G., Hartley, A. J., Grant, N. T. and Hodgkinson, R., Salt Tectonics, Sediments and Prospectivity. Geol Soc Spec Publ, 363, 33-57, https://doi.org/10.1144/SP363.3, 2012.

Rowan, M.G., Muñoz, J.A., Roca, E., Ferrer, O., Santolaria, P., Granado, P., Snidero, M.: Linked detachment folds, thrust faults, and salt diapirs: Observation and analog models, J Struct Geo, 155, 104509, https://doi.org/10.1016/j.jsg.2022.104509, 2022.

Rowan, M.G. and Ratliff, R.A.: Cross-section restoration of salt-related deformation: Best practices and potential pitfalls, J Struct Geo, 41, 24-37, https://doi.org/10.1016/j.jsg.2011.12.012, 2012.

Rowan, M.G., Urai, J., Fiduk, J.C., Kukla, P.A.: Deformation of intrasalt competent layers in different modes of salt tectonics, Solid Earth, 10, 987-1013, https://doi.org/10.5194/se-10-987-2019, 2019.

Rowan, M.G., Peel, F.J., Vendeville, B.C., Gaullier, V.: Salt tectonics at passive margins: Geology vs models – discussion, Mar Petrol Geol, 37, 184-194, https://doi.org/10.1016/j.marpetgeo.2012.04.007, 2012.

Santolaria, P., Ferrer, O., Rowan, M.G., Snidero, M., Carrer, N., Granado, P., Muñoz, J.A., Roca, E., Schneider, C.L., Piña, A., Zamora, G.: Influence of preexisting salt diapirs during thrust wedge evolution and secondary welding: Insights from analog modeling, J Struct Geo, 149, 104374, https://doi.org/10.1016/j.jsg.2021.104374, 2021.

Saura, E., Ardèvol i Oró, L., Teixell, A., Vergés, J.: Rising and falling diapirs, shifting depocenters and flap overturning in the Cretaceous Sopeira and Sant Gervàs subbasins (Ribagorça basin, Southern Pyrenees), Tectonics, 35, https://doi.org/10.1002/2015TC004001, 2016.

Schellart, W.: Shear test results for cohesion and friction coefficients for different granular materials: scaling implications for their usage in analogue modelling, Tectonophysics, 324, 1-16, https://doi.org/10.1016/S0040-1951(00)00111-6, 2000.

Scisciani, V., Agostini, S., Calamita, F., Pace, P., Cilli, A., Paltrinieri, W.: Positive inversion tectonics in foreland fold-and-thrust belts: A reappraisal of the Umbria–Marche Northern Apennines (Central Italy) by integrating geological and geophysical data, Tectonophysics, 637, 218-237, https://doi.org/10.1016/j.tecto.2014.10.010, 2014.

Stewart, S.A. and Clark, J.A.: Impact of salt on the structure of the Central North Sea hydrocarbon fairways, edited by: A. J. Fleet and S. A. R. Boldy, Petroleum Geology of Northwest Europe, Proceedings of the 5th Conference: Geological Society, London, 179-200, https://doi.org/10.1144/0050179, 1999.

Stewart, S.A.: Detachment-controlled triangle zones in extension and inversion tectonics. Interpretation, 2, 4, SM29-SM38, https://doi.org/10.1190/INT-2014-0026.1, 2014.

Talbot, C.J. and Aftabi, P.: Geology and models of salt extrusion at Qum Kuh, central Iran, J Geol Soc London, 161, 321-334, https://doi.org/10.1144/0016-764903-102, 2004.

Tari, G., Arbouille, D., Schléder, Z., Tóth, T.: Inversion tectonics: a brief petroleum industry perspective, Solid Earth, 11, 1865-1889, https://doi.org/10.5194/se-11-1865-2020, 2020.

Turner, J.P. and Williams, G.A.: Sedimentary basin inversion and intra-plate shortening. Earth Science Reviews, 65, 277-304, https://doi.org/10.1016/j.earscirev.2003.10.002, 2004.

Ventisette,C., Montanari, D., Bonini, M., Sani1, F.: Positive fault inversion triggering 'intrusive diapirism': an analogue modelling perspective, Terra Nova, 17, 478-485, https://doi.org/10.1111/j.1365-3121.2005.00637.x, 2005.

Vidal-Royo, O., Rowan, M.G., Ferrer, O., Fischer, M.P., Fiduk, J.C., Canova, D.P., Hearon, T.H., Giles, K., The transition from salt diapir to weld and thrust: Examples from the Northern Flinders Ranges in South Australia, Basin Res, 33, 2675-2705, https://doi.org/10.1111/bre.12579, 2021.

Warsitzka, M., Kely, J., and Kukowski, N.: Analogue experiments of salt flow and pillow growth due to basement faulting and differential loading, Solid Earth, 6, 9-31, https://doi.org/10.5194/se-6-9-2015, 2015.

Weijermars, R.: Flow behavior and physical chemistry bouncing putties and related polymers in view of tectonic laboratory applications, Tectonophysics, 124, 325-358, https://doi.org/10.1016/0040-1951(86)90208-8, 1986.

Weijermars, R., Jackson, M.P.A., Vendeville, B.: Rheological and tectonic modeling of salt provinces, Tectonophysics, 217, 143-174, https://doi.org/10.1016/0040-1951(93)90208-2, 1993.

Withjack, M.O. and Callaway, S.: Active normal faulting beneath a salt layer: an experimental study of deformation patterns in the cover sequence, AAPG Bull, 84, 627-651, DOI: 10.1306/C9EBCE73-1735-11D7-8645000102C1865D, 2000.

Withjack, M.O., Meisling, K.E., and Russell, L.R.: Forced folding and basement-detached normal faulting in the Haltenbanken Area, Offshore Norway: chapter 37: North Sea and Barents Shelf, edited by: Tankard, A.J., and Balkwill, H.R., Extensional Tectonics and Stratigraphy of the North Atlantic Margins, AAPG Memoir 46, 567-575, https://doi.org/10.1306/M46497C37, 1989.

Withjack, M.O., Schlische, R.W., Olsen, P.: Rift-basin structure and its influence on sedimentary systems, edited by: Renaut, R.W., Ashley, G.M., Sedimentation in Continental Rifts. SEPM Special Publication, 73, 57-81, 2002.

Yin, H. and Groshong, R.H.Jr.: Balancing and restoration of piercement structures: geologic insights from 3D kinematic models, J Struct Geo, 28, 99-114, https://doi.org/10.1016/j.jsg.2005.09.005, 2006.

https://doi.org/10.5194/egusphere-2022-1183
Preprint. Discussion started: 12 December 2022

Table 2. *Scaling parameters used in the experimental programme*

Parameter	Experiment	Nature	Model ratio
Thickness			
Pre-kinematic overburden	7.5 - 15 mm	750 - 1500 m	10^{-5}
Syn-kinematic overburden	0 - 33 mm	0 - 3300 m	10^{-5}
Salt/Polymer *	5 - 10 mm	500 - 1000 m	10^{-5}
Density			
Overburden	1500 kg m^{-3}	2700 kg m^{-3}	0.55
Salt/Polymer	972 kg m^{-3}	2200 kg m^{-3}	0.44
Density contrast	528	500	1.05
Ductile layer viscosity	1.6×10^{-4} Pa s	10^{-18} - 10^{-19} Pa s	1.6×10^{-14} - 1.6×10^{-15}
Overburden coefficient friction	0.7	0.8	0.87
Gravity acceleration	9.81 m s^{-2}	9.81 m s^{-2}	1

Thickness at the begining of the extension

Table 2. Scaling parameters used in the experimental program.

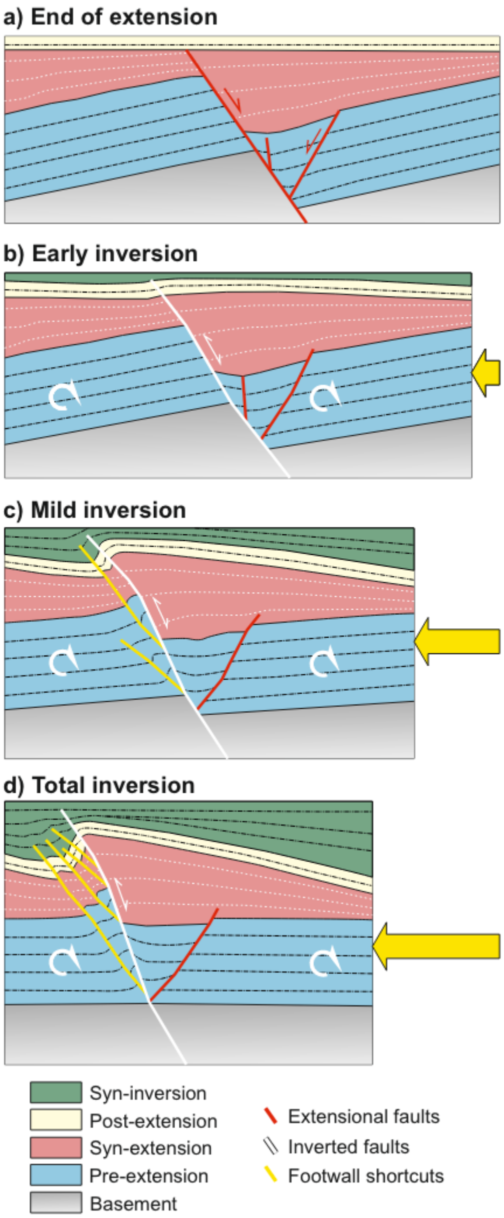

Figure 1. Schematic example of basin inversion of a domino-style basement fault lacking a decoupling layer. a) Structural configuration at the end of the extensional episode; b) early stage of inversion with the reactivation of the basement fault producing an incipient basin uplift; c) mild inversion stage and development of shortcuts affecting the whole sedimentary succession; and d) final configuration when total inversion is reached. Note the different distributions of the syn-kinematic depocenters (i.e., extension and inversion successions). Redrawn from an analogue model by Jagger and McClay (2018).

https://doi.org/10.5194/egusphere-2022-1183
Preprint. Discussion started: 12 December 2022

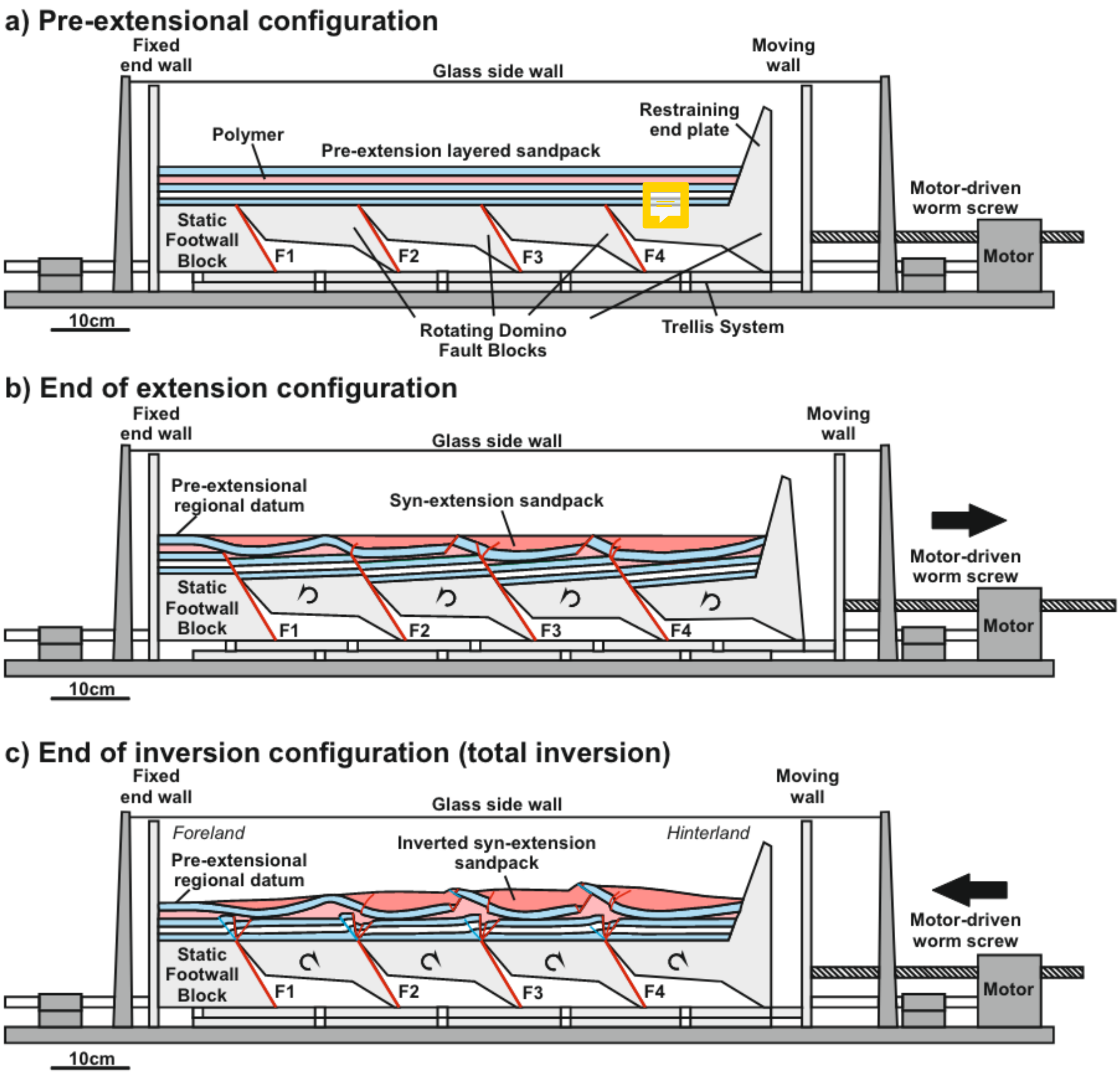

Figure 2. Sketch of the deformation rig used to simulate extension of domino-style basement fault system. a) Pre-extensional configuration and sedimentary infill characterised by a layered sand pack with an intervening polymer covering the entire model. b) Configuration at the end of extension characterised by a reddish syn-kinematic sand pack deposited as basement faults increase displacement. c) End of the compression configuration reaching total inversion.

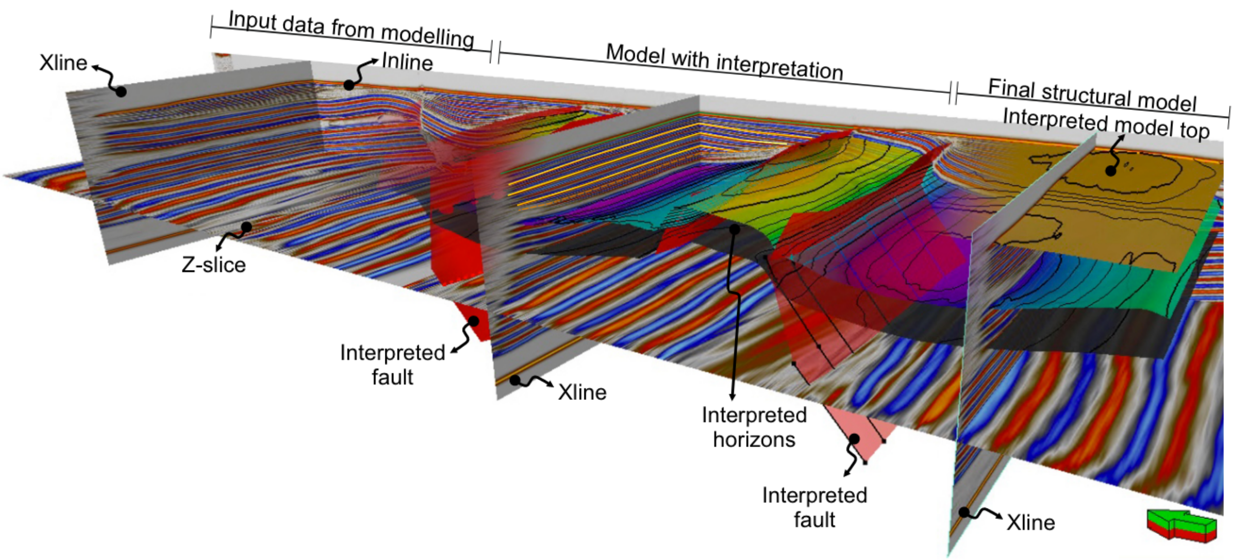

Figure 3. Example of a 3D SEGY generated from the vertical slices of the model showing the ability to display or hide the interpretation but also the final 3D structural model generated from the interpretation of the input data.

https://doi.org/10.5194/egusphere-2022-1183
Preprint. Discussion started: 12 December 2022

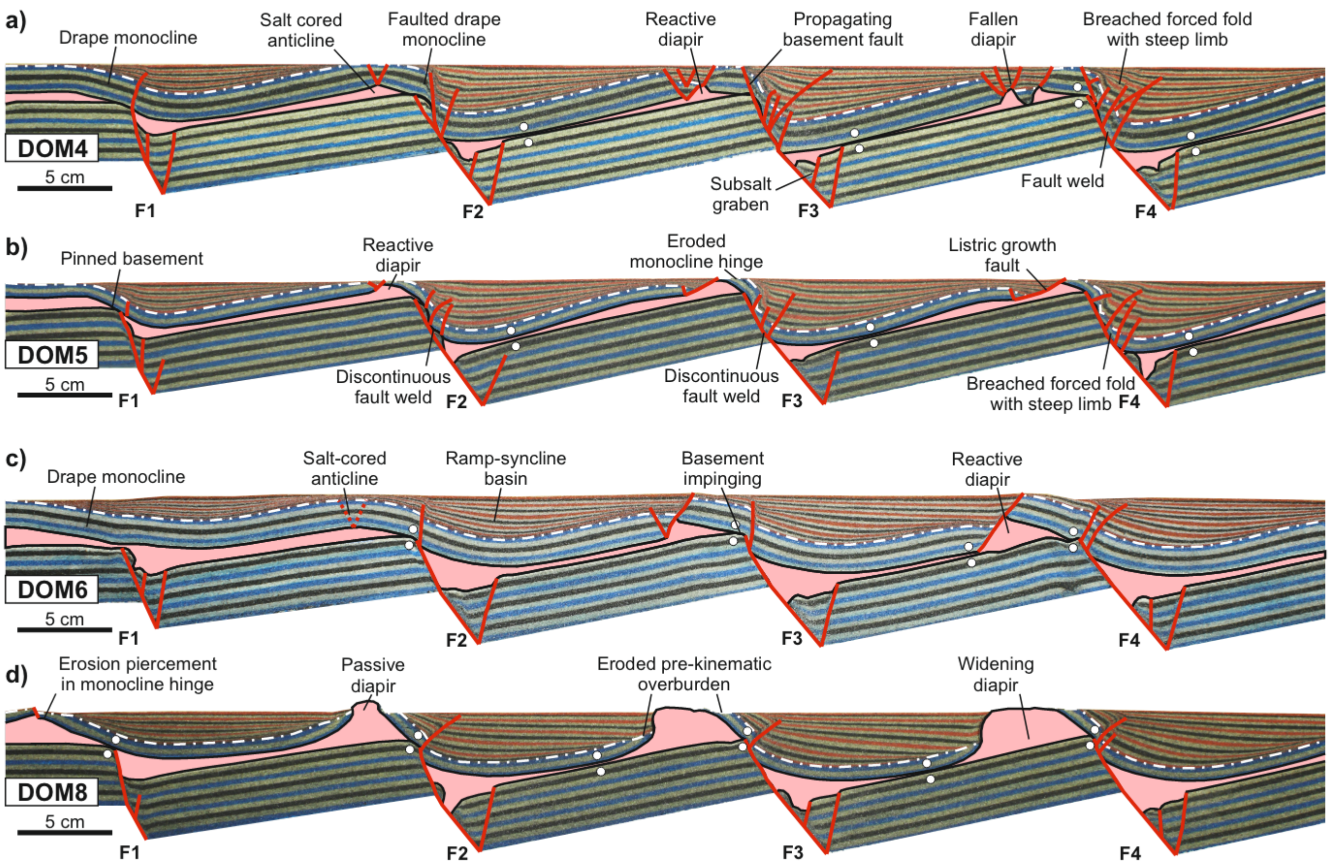

Figure 4. Central cross-section of the different extensional experiments illustrating the structural styles developed after 10 cm of extension (see parameters in Table 1). a) Model DOM4 (thin polymer – thick pre-kinematic overburden); b) Model DOM5 (thin polymer – thin pre-kinematic overburden); c) Model DOM6 (thick polymer – thick pre-kinematic overburden); and d) Model DOM8 (thick polymer – thin pre-kinematic overburden). Note how depending on the ratio between polymer and pre-kinematic overburden thicknesses results in the development of different salt-related structures but also different salt-detached ramp-syncline basin architectures.

https://doi.org/10.5194/egusphere-2022-1183
Preprint. Discussion started: 12 December 2022

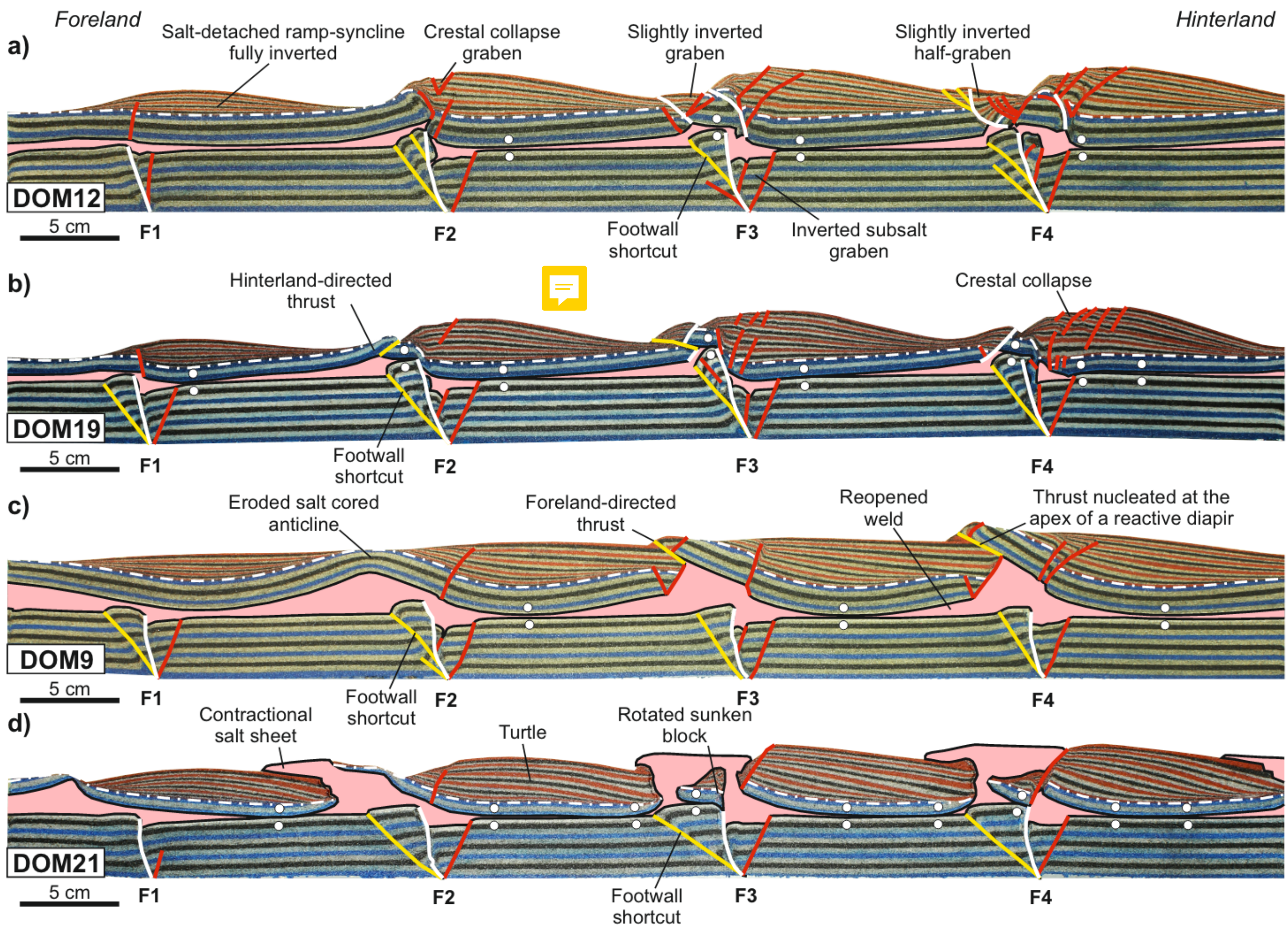

Figure 5. Central cross-section of the different compressional experiments illustrating the structural styles developed after total inversion (10 cm of shortening) (see parameters in Table 1). a) Model DOM12 (thin polymer – thick pre-kinematic overburden); b) Model DOM19 (thin polymer – thin pre-kinematic overburden); c) Model DOM9 (thick polymer – thick pre-kinematic overburden); and d) Model DOM21 (thick polymer – thin pre-kinematic overburden). The colors of the faults keep consistent with figure 1.

https://doi.org/10.5194/egusphere-2022-1183
Preprint. Discussion started: 12 December 2022

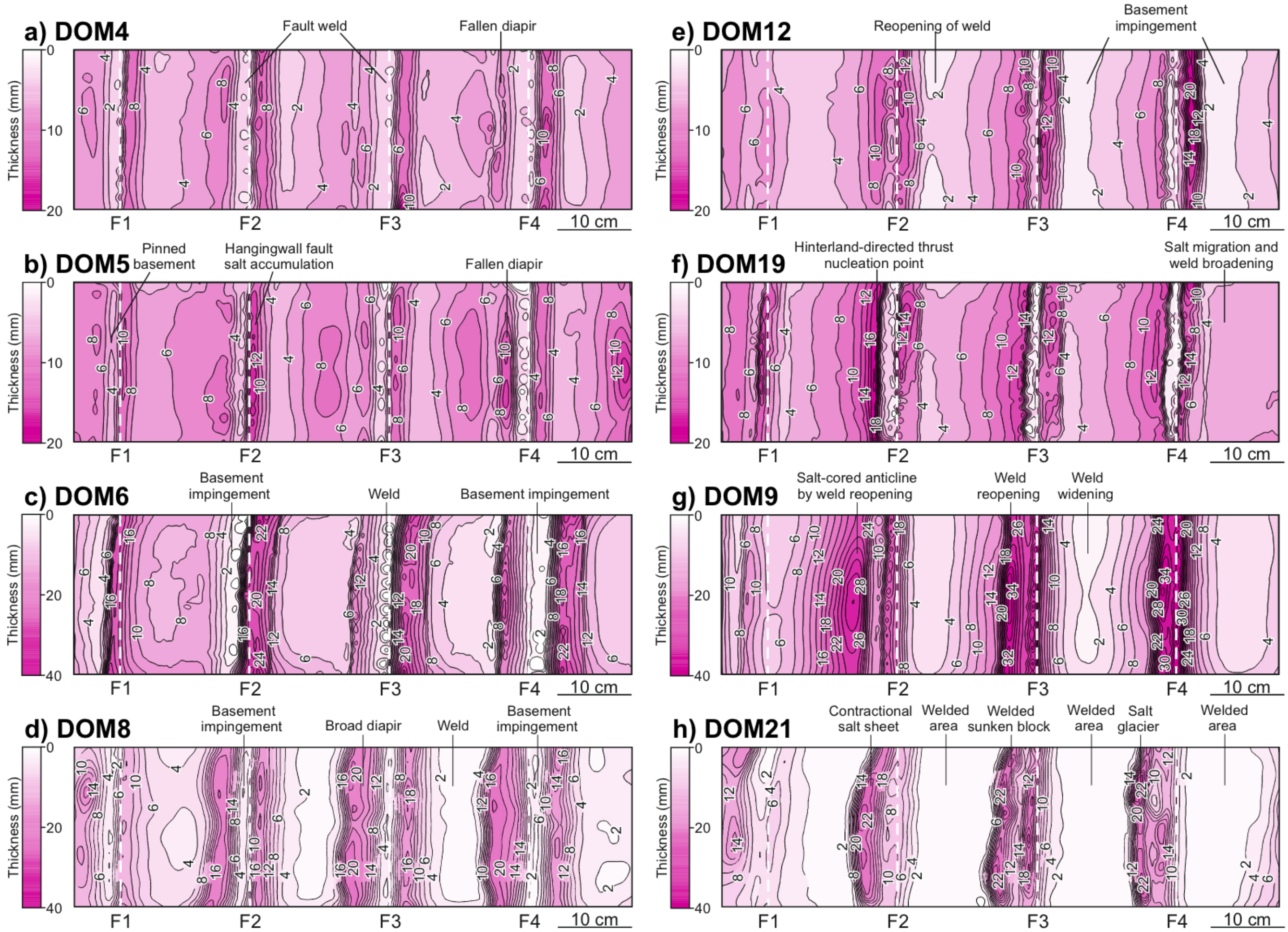

Figure 6. Isopach maps of the polymer level after extension (a to d) and after total inversion (e to h). Notice how the scale range in models DOM6, DOM8, DOM 9 and DOM21 (c, d, g and h) is double the range of the other models.

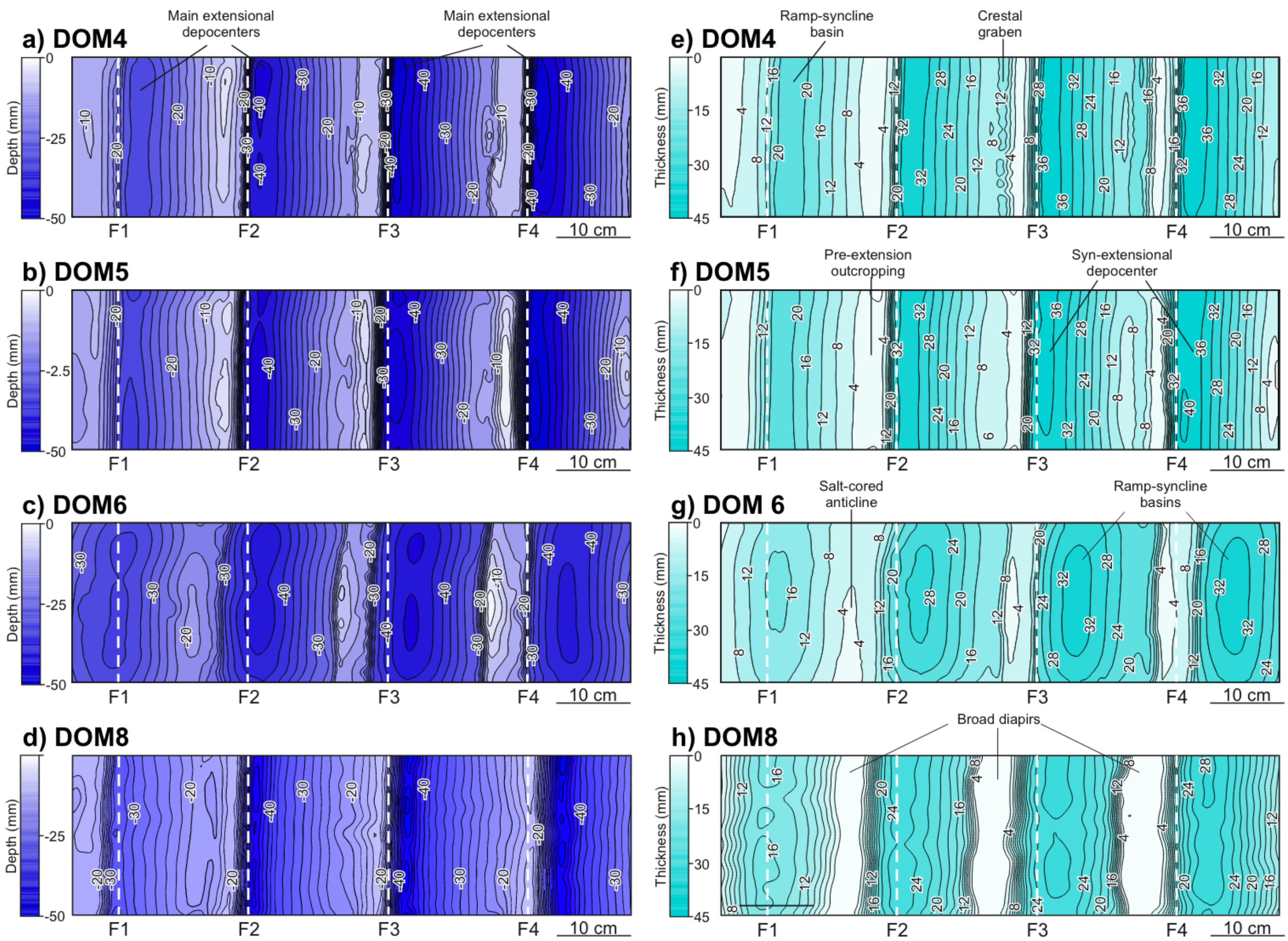

Figure 7. Isobath maps of the base of the salt at the end of extension (a to d) and isopach maps of the syn-extensional sequences at the end of extension (e to g).

https://doi.org/10.5194/egusphere-2022-1183
Preprint. Discussion started: 12 December 2022

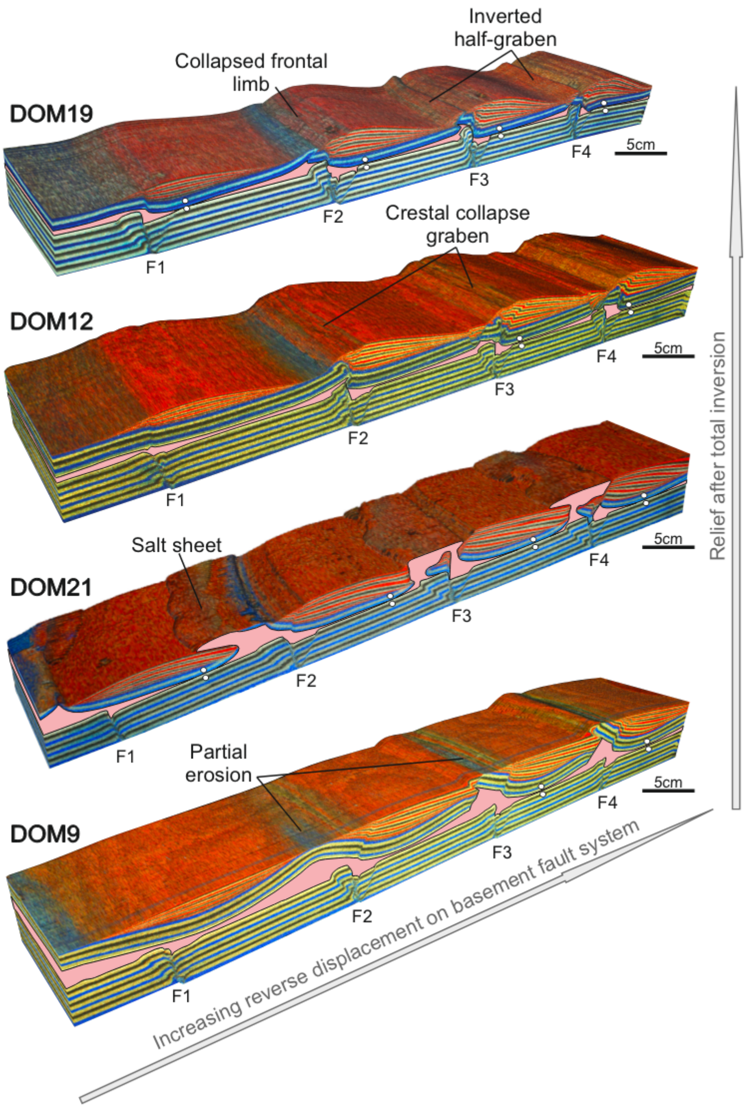

875 **Figure 8.** 3D Voxels of DOM19, DOM12, DOM21, DOM9 displaying the effect that the decoupling layer is having in the development of overburden structural relief after total inversion. Notice how faults close to the moving wall display more reverse displacement due to the apparatus design.

https://doi.org/10.5194/egusphere-2022-1183
Preprint. Discussion started: 12 December 2022

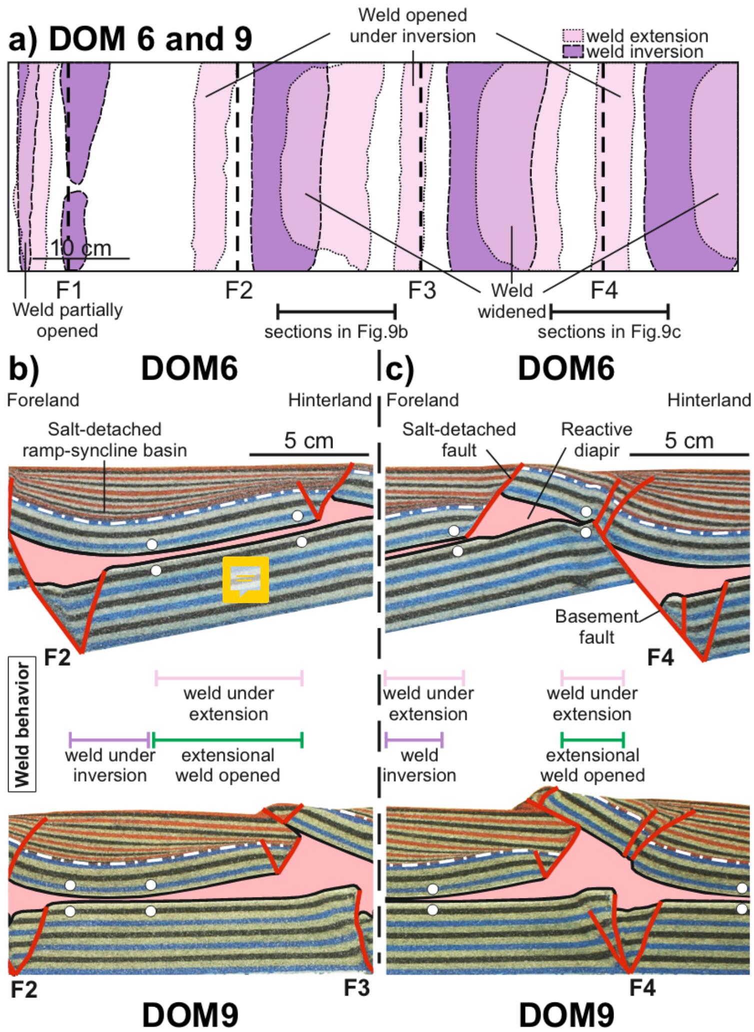

Figure 9. Weld reactivations. a) Map overlapping the weld distribution after extension and inversion. b) Weld reactivation example located below the salt-detached ramp-syncline basin. c) Weld reactivation example located above a basement extensional fault.

https://doi.org/10.5194/egusphere-2022-1183
Preprint. Discussion started: 12 December 2022

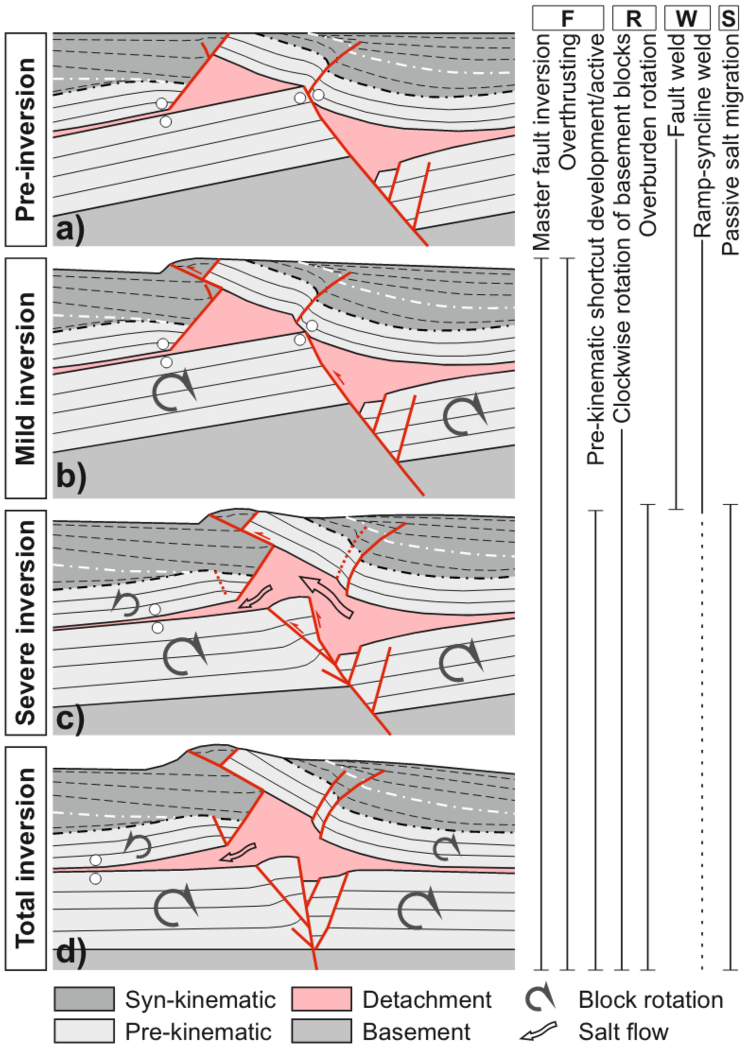

Figure 10. Sequential evolution of weld reopening from the post-extensional configuration to total inversion of a fault weld case example. F, R, W, S letters above the different processes correspond, respectively, to Fault (F); Rotations of sedimentary blocks (R); Welds (W); Salt migration (S).

https://doi.org/10.5194/egusphere-2022-1183
Preprint. Discussion started: 12 December 2022

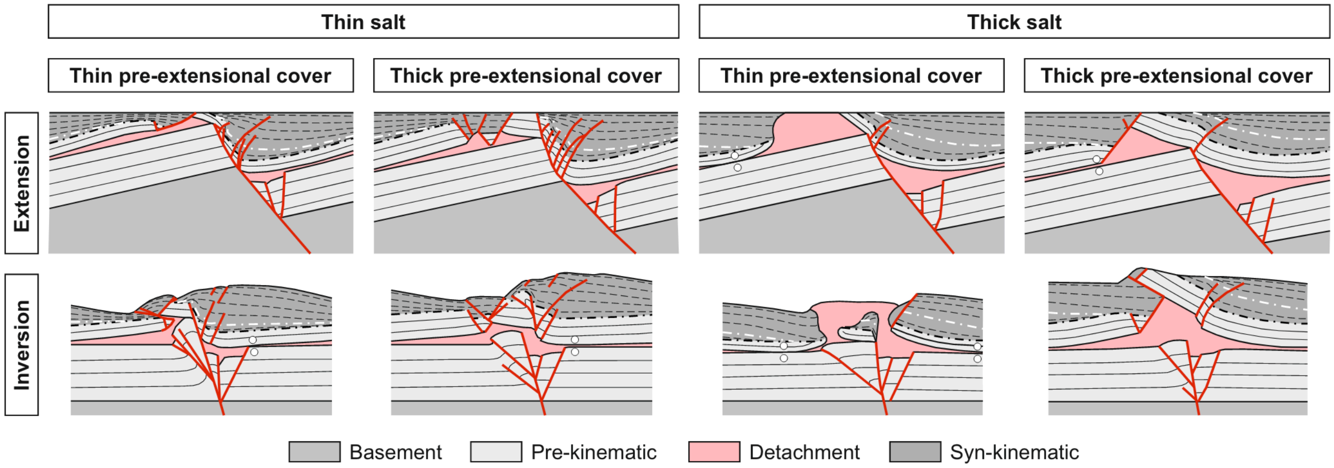

Figure 11. Summary figure displaying the different salt-related structural styles that resulted from extension and inversion of the different experimental configurations. Notice how the thickness of the salt layer (or its welded equivalent) conditions the coupling/decoupling of the overburden succession thus conditioning the structural style.

https://doi.org/10.5194/egusphere-2022-1183
Preprint. Discussion started: 12 December 2022

Table 1. *Experimental programme*

Model	Polymer thickness (mm)	Pre-extensional overburden thickness (mm)	Velocity rate (mm/h)	Extension (10cm)	Inversion (10cm)
DOM4	5	15	4.6	Yes	-
DOM12	5	15	4.6	Yes	Yes
DOM5	5	7.5	4.6	Yes	-
DOM19	5	7.5	4.6	Yes	Yes
DOM6	10	15	4.6	Yes	-
DOM9	10	15	4.6	Yes	Yes
DOM8	10	7.5	4.6	Yes	-
DOM21	10	7.5	4.6	Yes	Yes

Table 1. Summary table with the main characteristics of the experimental program included in this article.

https://doi.org/10.5194/egusphere-2022-1183
Preprint. Discussion started: 12 December 2022

Table 2. *Scaling parameters used in the experimental programme*

Parameter	Experiment	Nature	Model ratio
Thickness			
Pre-kinematic overburden	7.5 - 15 mm	750 - 1500 m	10^{-5}
Syn-kinematic overburden	0 - 33 mm	0 - 3300 m	10^{-5}
Salt/Polymer *	5 - 10 mm	500 - 1000 m	10^{-5}
Density			
Overburden	1500 kg m^{-3}	2700 kg m^{-3}	0.55
Salt/Polymer	972 kg m^{-3}	2200 kg m^{-3}	0.44
Density contrast	528	500	1.05
Ductile layer viscosity	1.6×10^{-4} Pa s	10^{-18} - 10^{-19} Pa s	1.6×10^{-14} - 1.6×10^{-15}
Overburden coefficient friction	0.7	0.8	0.87
Gravity acceleration	9.81 m s^{-2}	9.81 m s^{-2}	1

* *Thickness at the begining of the extension*

Table 2. Scaling parameters used in the experimental program.